journal

J. Am. Ceram. Soc., 90 [5] 1347–1364 (2007)
DOI: 10.1111/j.1551-2916.2007.01583.x

Refractory Diborides of Zirconium and Hafnium

William G. Fahrenholtz*,† and Gregory E. Hilmas*

Materials Science and Engineering Department, University of Missouri-Rolla, Rolla, Missouri 65409

Inna G. Talmy* and James A. Zaykoski*

Naval Surface Warfare Center, Carderock Division, West Bethesda, Maryland 20817

This paper reviews the crystal chemistry, synthesis, densification, microstructure, mechanical properties, and oxidation behavior of zirconium diboride (ZrB_2) and hafnium diboride (HfB_2) ceramics. The refractory diborides exhibit partial or complete solid solution with other transition metal diborides, which allows compositional tailoring of properties such as thermal expansion coefficient and hardness. Carbothermal reduction is the typical synthesis route, but reactive processes, solution methods, and pre-ceramic polymers can also be used. Typically, diborides are densified by hot pressing, but recently solid state and liquid phase sintering routes have been developed. Fine-grained ZrB_2 and HfB_2 have strengths of a few hundred MPa, which can increase to over 1 GPa with the addition of SiC. Pure diborides exhibit parabolic oxidation kinetics at temperatures below 1100°C, but B_2O_3 volatility leads to rapid, linear oxidation kinetics above that temperature. The addition of silica scale formers such as SiC or $MoSi_2$ improves the oxidation behavior above 1100°C. Based on their unique combination of properties, ZrB_2 and HfB_2 ceramics are candidates for use in the extreme environments associated with hypersonic flight, atmospheric re-entry, and rocket propulsion.

I. Introduction

Zirconium diboride (ZrB_2) and hafnium diboride (HfB_2) are members of a family of materials known as ultra high-temperature ceramics (UHTCs). Several carbides and nitrides of the group IVB and VB transition metals are also considered UHTCs based on melting temperatures in excess of 3000°C and other properties. Very few elements or compounds from any class of ceramic materials have melting temperatures approaching 3000°C (Fig. 1).[1] From the broader family of UHTCs, this paper focuses on ZrB_2 and HfB_2. Discussion of TiB_2 has been intentionally minimized due to its more widespread use as armor and cutting tools.[2–4]

Some structural, physical, transport, and thermodynamic properties of ZrB_2 and HfB_2 are summarized in Table I.[5–12] Applications that take advantage of these properties include refractory linings,[13–15] electrodes,[16–18] microelectronics,[19] and cutting tools.[20] In addition to high melting temperatures, ZrB_2 and HfB_2 have a unique combination of chemical stability, high electrical and thermal conductivities, and resistance to erosion/corrosion that makes them suitable for the extreme chemical and thermal environments associated with hypersonic flight, atmospheric re-entry, and rocket propulsion.[21–24] Because of recent efforts to develop hypersonic aerospace vehicles and re-usable atmospheric re-entry vehicles, interest in UHTCs has increased significantly in the past few years. As a result, groups in the United States, Italy, Japan, India, and China are investigating diborides. Many of these studies draw inspiration from the late Professor G. V. Samsonov, whose work is noted for both its high quality and enormous quantity.

This article provides a critical evaluation of historic (1970s or earlier) and recent (1990 or later) studies of ZrB_2 and HfB_2 ceramics as well as presenting some recent results. Fundamental aspects of crystal structure and bonding, synthesis, densification, microstructures, properties, and oxidation behavior are examined.

II. Crystal Structure and Bonding

Crystal chemistry and crystal structure determine the chemical, physical, and thermal properties of materials. For the transition metal diborides, fundamental aspects of crystal structure and crystal chemistry have been discussed extensively dating to the early 1950s.[25–46] This section reviews the bonding, structure, structure-property relations, and solid solutions of the diborides.

(1) Bonding and Structure

Borides have a wide range of compositions with boron:metal (B:M) ratios ranging from 1:4 to 12:1. The B:M ratio affects both properties and electronic structure. Changing B:M changes the electronic structure of boron, which leads to the formation of different structural complexes containing one-, two-, and three-dimensional (3D) B networks. Increasing the number of

D. Green—contributing editor

Manuscript No. 22451. Received November 6, 2006; approved January 10, 2007.
At UMR, portions of this work were funded by the Air Force Office of Scientific Research (F49620-03-1-0072 and FA9550-06-1-0125), the National Science Foundation (DMR-0346800), and the Air Force Research Laboratory (FA8650-04-C-5704). At NSWCCD the work was funded by the Office of Naval Research on several contracts monitored by Dr. Steve Fishman.
*Member, American Ceramic Society.
†Author to whom correspondence should be addressed. e-mail: billf@umr.edu

Feature

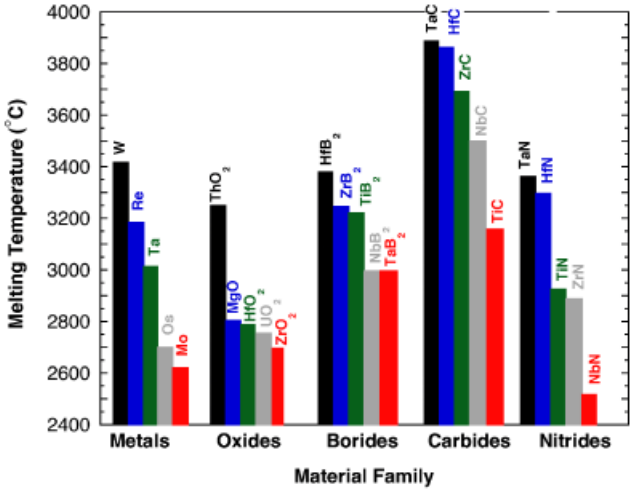

Fig. 1. A comparison of the melting temperatures of the most refractory members of several classes of materials. Several borides, carbides, and nitrides have melting temperatures above 3000°C and are considered ultra high-temperature ceramics. For comparison, the melting temperature of Zr is ~1850°C and the melting temperature of Hf is ~2227°C.

B atoms in a structural complex leads to increases in the B–B bond strength and an increase in the stiffness of the crystal lattice along with increases in melting temperature (T_m), hardness (H_V), strength (σ), and chemical stability.

The M–B bond strength in diborides depends on the degree of electron localization around the M atoms. The valence electron configuration in isolated B atoms is $2s^2 2p$. In metal borides, the outer electron configurations are sp^2 and sp^3, which promote strong covalent bonding. In diborides, B atoms are electron acceptors, while the M atoms are electron donors. Each M atom donates two electrons (one to each B), which converts M to a doubly charged cation, while B atoms become singly charged anions. So, the MB_2 formula can be expressed $M^{2+}(B^-)_2$.[31,32,40–45] The electron configurations vary depending on the donor properties of M, which produces a diversity of crystal structure types and properties. The M–B bonds have ionic characteristics as a result of the donor–acceptor interactions, but they also have covalent characteristics due to partial excitation of *d* electrons and the formation of *spd* hybrid configurations. The tendency for B atoms to form sp^2 and sp^3 hybrids also affects properties.

Table I. Summary of Some Structural, Physical, Transport, and Thermodynamic Properties of ZrB_2 and HfB_2

Property	ZrB_2	HfB_2
Crystal system space group	Hexagonal[5]	Hexagonal[6]
prototype structure	*P6/mmm* AlB_2	*P6/mmm* AlB_2
a (Å)	3.17	3.139
c (Å)	3.53	3.473
Density (g/cm^3)	6.119[5]	11.212[6]
Melting temperature (°C)	3245[1]	3380[1]
Young's modulus (GPa)	489[9]	480[11]
Bulk modulus (GPa)	215	212
Hardness (GPa)	23[9]	28[7]
Coefficient of thermal expansion (K^{-1})	5.9×10^{-6} [7]	6.3×10^{-6} [7]
Heat capacity at 25°C ($J \cdot (mol \cdot K)^{-1}$)	48.2[8]	49.5[7]
Electrical conductivity (S/m)	1.0×10^{7} [7]	9.1×10^{6} [7]
Thermal conductivity ($W \cdot (m \cdot K)^{-1}$)	60[7]	104[9]
Enthalpy of formation at 25°C (kJ)	−322.6[8]	−358.1[7]
Free energy of formation at 25°C (kJ)	−318.2[8]	−332.2[7]

However, hardness and brittleness are lower than the corresponding carbides because the B structural complexes combine sp^3 hybridization with the lower-strength sp^2 (and even lower-strength s^2p and *sp*) configurations, whereas the carbon atoms in carbides exhibit only sp^3 hybridization.

As shown in Fig. 2, the crystal structure of Group IV–VI transition metal diborides is primitive hexagonal (AlB_2-type, *P6/mmm* space group). The unit cell contains one MB_2 formula unit. The structure is composed of layers of B atoms in 2D graphite-like rings or nets, which alternate with hexagonally close-packed M layers. Each M atom is surrounded by six equidistant M neighbors in its plane and 12 equidistant B neighbors (six above and six below the M layer). Each B is surrounded by three B neighbors in its plane and by six M atoms (three above and three below the B layer).

The unit-cell parameters and interatomic distances for diborides are summarized in Table II. In general, B–B separation controls the *a*-axis length. However, the *a*-axis length is also affected by M–B contact. For ZrB_2, which has the largest M atom of the diborides, the B–B distance is 1.83 Å ($a/\sqrt{3}$), which exceeds the "normal" B–B distance (1.74 Å) by 0.09 Å due to stretching of the B–B bonds by Zr–Zr contact. Likewise, the smallest M atoms (Cr, V) lead to reductions in the B–B distance. From crystal chemical considerations, the length of the *a*-axis is a balance between two forces: (1) repulsion between atoms in the M layers and (2) attraction between atoms in the B nets.[26,29,30] As a result, stable AlB_2-type diborides do not form for M atoms smaller than Cr or larger than Zr. The B–B bond length for minimum strain in the boron nets has been estimated to be ~1.75Å, which is the value for TiB_2.[29]

The M–B distance in diborides increases linearly with the M:B radius ratio, increasing from 2.30 Å for CrB_2 to 2.54 Å for ZrB_2. The M–B separation is equal to $(a^2/3 + c^2/4)^{1/2}$, which is larger than the sum of the M and B radii (Table II). Generally, the structural data indicate that bonding in the B nets controls the lattice parameters in the AlB_2-type structure. Because the B–B bonds are strong relative to the other bonds, increases in the *a*-axis with increasing M size are minimal. In contrast, no such effect is observed for the *c*-axis. Hence, the *c*:*a* ratio increases with increasing M atom size. Owing to separation of the close-packed M planes by B nets, the *c*-axis is always substantially larger than $2R_M$. In summary, differences among diborides result from different M radii, which lead to variations in the interatomic bond lengths. Larger changes are observed for the *c*-axis than for the *a*-axis due to the relative bond strengths.

(2) Structure-Property Relations

Hardness, bulk modulus, Debye temperature (Θ_D), T_m, coefficient of thermal expansion (CTE), thermal conductivity (*k*), and enthalpy of formation (ΔH_f^o) are some properties that are related to bond strength (cohesive energy). Generally, the combination of bonds (M–M, B–B, and M–B) influences the material properties. However, in some cases, a specific type of bond controls a property.[31] For example, B–B and M–B bonds in diborides control hardness and thermal stability. Hardness is, therefore, a qualitative indicator of bond strength.[47]

The thermal and elastic properties of diborides are summarized in Table III.[48–54] The data indicate that the Group IV diborides have lower CTE and higher Young's modulus and thermal conductivity than Group V diborides.[26] The property changes suggest that B–B bonds are strongest for Group IV atoms (Ti, Zr, and Hf) and the bonds weaken as atomic number increases across a period of the Periodic Table. Grimvall and Guillermet[46] found it useful to correlate cohesive energy and T_m trends to the average number of valence electrons per atom for isostructural diborides. For example, the series ScB_2, TiB_2, VB_2, CrB_2, MnB_2, and FeB_2 have 9, 10, 11, 12, 13, and 14 valence electrons, respectively. With its 10 valence electrons (3.3 electrons per atom), TiB_2 possesses the highest melting temperature of the group. Higher or lower numbers of valence electrons result in lower melting temperatures.

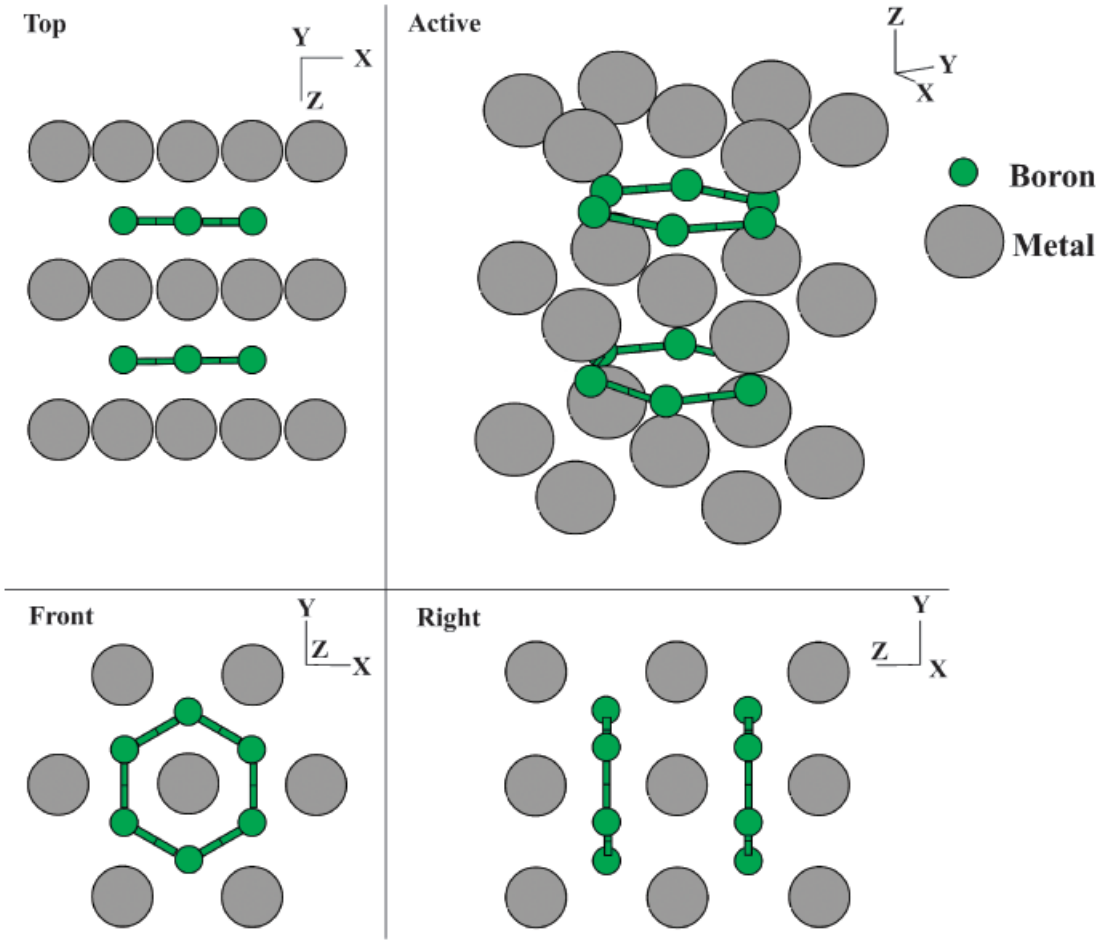

Fig. 2. Projections of the AlB_2-type structure. Pictures are taken from the Crystal Lattice Structures Web page, provided by the Center for Computational Materials Science of the United States Naval Research Laboratory.

Hardness can also be related to electronic structure despite wide differences in published data. The hardness of diborides decreases as the atomic number of the metal increases for Groups III–VI and Periods 4–6 of the Periodic Table. The Fermi level for ZrB_2 is located in a pseudogap between the completely occupied bonding states and free antibonding states. As a result, ZrB_2 has the maximum stability and microhardness for its period. Likewise, TiB_2 and HfB_2, which are isoelectronic and isostructural, have the highest hardness among their periods. For Group V diborides, a considerable number of valence electrons enter antibonding states, leading to decreases in bond strength and microhardness.[35] Hardness for TiB_2, ZrB_2, and HfB_2 decrease as temperature increases.[55]

The bonding in diborides also influences the anisotropy in properties. Microhardness measurements for TiB_2 conducted by Vehldiek[52] did not reveal any significant anisotropy in hardness along the *a*- or *c*-axes. In comparison, the Young modulus showed a high degree of anisotropy in some diborides.[53] Estimation of stresses from strain-induced broadening of X-ray diffraction (XRD) peaks revealed that the Young's moduli of TiB_2 and ZrB_2 were reasonably isotropic, while NbB_2 was extremely anisotropic, with lower values observed for the [00*l*] direction.[56] This behavior is observed in structures where the bonds are weaker in one direction than for other directions. Based on line broadening studies, it was concluded that TiB_2 had strong bonding in all directions, bonding in ZrB_2 was isotropic, but weaker than in TiB_2, and that NbB_2 was highly anisotropic with weak bonding between (00*l*) planes.

Table II. Unit Cell Parameters and Interatomic Distances in Diborides[26,30]

Metal boride	Size or length (Å)						
	c/*a*	*c*	*a*	R_M^0	B–B	M–B	$2R_M^0 + R_B$
ZrB_2	1.114	3.530	3.169	1.61	1.830	2.54	2.48
HfB_2	1.105	3.470	3.141	1.58	1.813	2.51	2.46
TaB_2	1.041	3.225	3.097	1.49	1.788	2.41	2.36
NbB_2	1.05	3.27	3.11	1.48	1.79	2.43	2.36
TiB_2	1.064	3.228	3.028	1.47	1.748	2.38	2.34
CrB_2	1.030	3.066	2.969	1.30	1.714	2.30	2.18

R_M^0 is the metal radius and R_B is the radius of boron.

Post *et al.*[30] were first to show that diborides with metals of large radii had the highest melting temperatures. Because the B–B separations are the highest and the B–B bonds are the weakest for the highest melting temperature diborides, the authors came to the conclusion that the M–B bond strength was responsible for melting temperatures.

The CTEs of various diborides have been measured.[57–59] Using XRD analysis up to 1600°C, Keihn and Keplin[57] showed that ZrB_2 and HfB_2 had lower CTE anisotropy than the diborides of Ti, Nb, and Ta. The authors concluded that polycrystalline ZrB_2 and HfB_2 ceramics would develop lower internal stresses during rapid cooling than other diborides. With the exception of CrB_2, the lattice parameters and CTEs of the diborides had similar temperature dependences for the *a*- and *c*-axes, which indicates little anisotropy in the bond strength in the two directions. The CTE in the *c*-direction decreases with increasing M radius, which can be correlated with an increase in the M–B bond strength with increasing M size. The CTE in the *a*-direction does not change significantly with increasing M radius. Taken together, the results can be interpreted to indicate that the B–B bonds determine the cohesive forces in the *a*-direction, while weaker M–B bonds control cohesive behavior in the *c*-direction.[59]

Table III. Thermal and Elastic Parameters of Transition Metal Borides[26]

Boride	CTE (ppm/K)	Θ_D (K) Calc. from α	Θ_D (K) Calc from T_M	E (GPa)	H_V (GPa)	k W·(m·K)$^{-1}$
TiB_2	4.8	1100	970	530	13	20.6
ZrB_2	6.2	765	730	420	15	18.9
HfB_2	6.6	550	580	—	—	16.6
VB_2	8.0	880	880	340	—	13.1
NbB_2	8.2	701	720	—	—	6.9
TaB_2	8.5	545	570	280	—	6.0
CrB_2	10.5	726	780	220	13	31.8

(3) Solid Solubility

Mutual continuous solid solutions form among Group IV and V diborides. Because their radii differ by $<10\%$, HfB_2 and ZrB_2 form continuous solid solutions with TiB_2, NbB_2, and TaB_2. A larger radius difference leads to limited solubility between these diborides and CrB_2.[25,30] The activation energy for the formation of diboride solid solutions is essentially the same as the activation energy for M diffusion. For example, the activation energies for the formation of solid solutions in the ZrB_2–TiB_2 and TiB_2–NbB_2 systems are 175 and 112 kJ/mol, respectively, which correspond to the activation energies for metal diffusion in these systems. In comparison, the NbB_2–CrB_2 system exhibits higher values for activation energy (400 kJ/mol), which can be attributed to the large disparity in atomic radii between Nb and Cr (13%) compared with Zr and Ti (9%) or Ti and Nb (1%). Based on activation energy data, solid solution formation appears to depend on diffusion of M atoms, not the strongly bonded B atoms.

Some diboride solid solutions show deviations from "rule of mixture" predictions for properties such as hardness and electrical conductivity, although some changes are only observed over limited composition ranges that are specific to each system. For example, TiB_2–ZrB_2 solid solutions exhibited a maximum in hardness between 30 and 70 mol% ZrB_2. The hardness at 50 mol% ZrB_2 was 24 GPa compared with values of 18 GPa for TiB_2 and 12 GPa for ZrB_2 as reported in the study.[60] For TiB_2–ZrB_2 ceramics synthesized by a combustion synthesis-microwave process followed by hot pressing (HP), the highest values of relative density (99%), flexure strength (680 MPa), fracture toughness (7.3 MPa·m$^{1/2}$), and hardness (27 GPa) were observed at 20% ZrB_2.[61] In another study, TiB_2–ZrB_2 ceramics containing 40 mol% ZrB_2 had the highest hardness (30.4 GPa), flexure strength (354 MPa), fracture toughness (3.87 MPa·m$^{1/2}$), Young's modulus (449 GPa), and fracture energy (16.5 J/m^2).[62] Local maxima in hardness have also been observed in other systems such as TiB_2–NbB_2 (at $\sim$38 mol% NbB_2),[63] NbB_2–CrB_2 (30 GPa at 80 mol% CrB_2),[64,65] and TiB_2–CrB_2 (at $\sim$20 mol%CrB_2).[66]

The lattice constants of diboride solutions show a linear dependence on composition in many systems. However, based on bonding considerations discussed above, *c*-axis parameters are more strongly affected by changes in composition than *a*-axis parameters. For TiB_2–WB_2 solid solutions with WB_2 contents between 40 and 60 mol%, the *a* parameter decreased only slightly as WB_2 content increased, whereas the *c* parameter exhibited a significant decrease.[67] For TiB_2–CrB_2 and TiB_2–ZrB_2 solutions, Zdaniewski[68] found that the degrees of lattice contraction (for Cr) or expansion (for Zr) were smaller than expected based on the sizes and concentrations of the M atoms. This suggests stronger interactions between the M and B atoms than would be expected from the M size alone and is likely due to differences in electron configurations and bond strength.[35,40] Changes in lattice anisotropy and elastic strain energy in solid solutions may also affect grain-boundary cohesion in polycrystalline ceramics.[68] If true, then knowledge of lattice parameter changes with composition could be used to improve the mechanical behavior of diboride ceramics by using compositional changes to induce beneficial stresses (for example, surface compression stresses).

Fendler *et al.*[69] studied thermal expansion of TiB_2–CrB_2 and TiB_2–WB_2 solid solutions using high-temperature XRD analysis. The CTEs of TiB_2–CrB_2 did not follow predictions from rule of mixtures calculations. The *c*-parameter exhibited an unexpected increase with temperature. For TiB_2–WB_2 solid solutions, the CTE was lower than TiB_2 at low temperatures.

Using experimental hardness values obtained from solid solutions as a function of composition,[61,64,66] NSWCCD researchers calculated the B–B bond lengths for compositions showing the maximum hardness in TiB_2–CrB_2, NbB_2–CrB_2, and TiB_2–ZrB_2 solid solutions. The B–B bond lengths were calculated to be 1.74, 1.73, and 1.75 Å, respectively. The values were similar to 1.75 Å, which Hughes and Hoard[29] suggested as the B–B bond length for minimum stress in the boron net. The result is also consistent with hardness values from pure diborides, which were higher for borides with the largest M atoms.

III. Synthesis

The diborides can be synthesized by a variety of routes. This section focuses on three main synthesis routes: (1) reduction processes, (2) chemical routes, and (3) reactive processes.

(1) Reduction Processes

Several reduction processes are used to synthesize diborides. Carbon and boron are the most common reducing agents, but boron carbide (B_4C) or aluminum (Al) can also be used as well as combinations of reducing agents.[70] Examples of the reactions used to synthesize diborides are shown in Table IV (Reactions (1)–(5)). These reactions were written for ZrB_2, but analogous processes produce HfB_2 or other diborides.

Carbothermal reduction is used to produce ZrB_2 and HfB_2 commercially.[71–73] The process is strongly endothermic; Reaction (1) has an enthalpy of reaction (ΔH^o_{rxn}) of 1475.6 kJ at 298 K. As a result, Reaction (1) is only thermodynamically favorable (i.e., $\Delta G^o_{rxn} < 0$) above $\sim$1500°C (Table IV). Based on reaction favorability and the heat absorbed, temperatures of $\sim$2000°C are generally employed to synthesize diborides.[71,74] The reactions also produce significant volumes of various gases, which must be removed for the reactions to proceed to completion. Excess B_2O_3 is often added to promote formation of diborides over carbides. Along with B_2O_3 and carbides, carbon is also a common impurity in the final powder.[70]

Table IV. Examples of Reduction Reactions that can be Used to Synthesize Borides and the Change in Free Energy of Reaction (ΔG^o_{rxn}) as a Function of Temperature

Reactions	Category	Example	(ΔG^o_{rxn}) (kJ)
(1)	Carbothermal	$ZrO_2(c) + B_2O_3(l) + 5C(g) \rightarrow ZrB_2(cr) + 5CO(g)$	1431–0.803T
(2)	Borothermal	$ZrO_2(c) + 4B(c) \rightarrow ZrB_2(c) + B_2O_2(g)$	301–0.178T
(3)	Aluminothermal	$3ZrO_2(c) + 3B_2O_3(l) + 10Al(l) \rightarrow 3ZrB_2(c) + 5Al_2O_3(c)$	−2412+0.495T
(4)	Boron Carbide	$7ZrO_2(c) + 5B_4C(c) \rightarrow 7ZrB_2(c) + 3B_2O_3(g) + 5CO(g)$	1378–0.924T
(5)	Combined	$2ZrO_2(c) + B_4C(c) + 3C(g) \rightarrow 2ZrB_2(c) + 4CO(g)$	1134–0.668T

Reduction with B_4C have also been used to produce diborides and diboride composites.[70–73,75] Like other reduction processes, the reactions between oxides and B_4C are endothermic. However, these reactions become favorable at temperatures lower than the corresponding reactions with carbon. For example, Reaction 4 becomes favorable around 1200°C whereas Reactions (1), (2), and (5) are only favorable above 1400°C (Table IV). Processes similar to Reaction (4) offer the additional benefit of reduced levels of carbon, B_2O_3, and oxide impurities in the reaction products. Reaction (4) has also been exploited to promote densification of B_4C and ZrB_2 based on the ability of B_4C to react with oxides and thereby reduce the amount of oxide impurities in non-oxide ceramics.[76,77]

(2) Chemical Routes

Chemical routes used to produce diborides include solutions, reactions with boron-containing polymers, and pre-ceramic polymers. Nanocrystalline ZrB_2 and HfB_2 have been synthesized by reacting anhydrous chlorides with sodium borohydride ($NaBH_4$) above 500°C under pressure.[78,79] The overall process is described by Reaction (6), but the reaction may proceed by a vapor phase mechanism that involves the decomposition of $NaBH_4$ to borane (BH_3) and its subsequent reaction with a gaseous chloride. Diborides prepared by these routes can have crystallite sizes as small as 10–20 nm[78,79]:

$$HfCl_4(g) + NaBH_4(g) \rightarrow HfB_2(c) + 2NaCl(c) + 2HCl(g) + 3H_2(g) \quad (6)$$

Titanium diboride has also been prepared by thermal decomposition of titanium borohydride (Reaction (7)). Powders prepared by this method were also nano-sized with diameters of 100–200 nm[80]:

$$2Ti(BH_4)_3(c) \rightarrow 2TiB_2(c) + B_2H_6(g) + 9H_2(g) \quad (7)$$

Nano-crystalline oxides produced by precipitation could be converted to diborides using reduction processes (Table IV). Sacks *et al.*[81] synthesized nano-crystalline ZrC and HfC by carbothermal reduction of ZrO_2 and HfO_2 produced by a sol–gel process. Similar processes should also work for nano-crystalline diborides, but, to date, only conventional micro-sized oxides have been converted to diborides.[82] A pre-ceramic polymer has been directly converted to a refractory diboride,[83] but the polymer was used as a binder for commercial ZrB_2 powder, not to produce a stand-alone coating or a monolithic ceramic. Finally, diboride-based composites have been prepared by combining conventional diboride powders with SiC-bearing pre-ceramic polymers such as polycarbosilane.[84,85] From these reports, a variety of chemical synthesis methods are available, but the processing of these powders into coatings or ceramics has not been fully explored.

(3) Reactive Processes

The simplest reaction synthesis method for producing diborides is the reaction of elemental precursor powders:

$$Zr + 2B \rightarrow ZrB_2 \quad (8)$$

$$Hf + 2B \rightarrow HfB_2 \quad (9)$$

The use of direct reactions dates back over 100 years, although pure diborides were not produced until nearly 50 years later due to the difficulty in obtaining high-purity boron.[70] The high oxygen affinity of both Zr and Hf means that the reactions must be carried out in inert or reducing atmospheres to prevent the formation of oxide impurities.

Reactions (8) and (9) are both extremely exothermic ($\Delta H^{\circ}_{rxn} = -323$ and -328kJ, respectively, at 298 K) and favorable at all temperatures.[10,86] If allowed to proceed in an uncontrolled manner, the heat can ignite a self-propagating reaction and generate temperatures high enough to promote local melting of the Zr ($T_m = \sim 1850$°C) or Hf ($T_m = \sim 2225$°C).[87] Thus, Reactions (8) and (9) can be used to synthesize ZrB_2 and HfB_2 by self-propagating high-temperature synthesis (SHS), which is also known as combustion synthesis.[88–90] The high heating and cooling rates associated with SHS produce high defect concentrations in the resulting diborides, which have been linked to improved sinterability of SHS-derived powders.[91] The SHS method also lends itself to preparation of diboride-containing composites or diborides doped with additives such as sintering aids.[92,93] In addition, a great deal of work has been done on SHS of TiB_2 ceramics, all of which is directly applicable to ZrB_2 and HfB_2.

In contrast to SHS, recent research at UMR has employed slow heating (~1°C/min) and extended isothermal holds (6 h at 600°C) to react fine powders of Zr and B without the ignition of SHS reactions.[94] Under controlled heating, Zr and B react to form phase-pure ZrB_2 at temperatures as low as 600°C. The ZrB_2 crystallites produced by controlled reactions were the same size as the Zr precursor particles. Hence, reduction of the starting Zr particle size before reaction reduced the size of the resulting ZrB_2. Analysis showed that the crystallite size of ZrB_2 formed from Zr attrition milled for 240 min was ~10 nm. Particles coarsened significantly as temperature increased and grew to more than 1 μm at 1650°C (Table V). Coarsening in non-oxides ceramics, including diborides, is promoted by oxygen present as oxide impurities on the particle surfaces.[3,77,95,96] A significant amount of oxygen (2.4 wt%) was detected in ZrB_2 produced by Reaction (8), which was higher than reported for conventional powders (0.9% for as received H. C. Starck Grade B powder, 2.0 wt% after attrition milling for 2 h in hexane).

Table V. Crystallite/Grain Size and Density for ZrB_2 and ZrB_2–SiC Produced by Reactive Hot Pressing of Zr-B and Zr–B–SiC Powder Mixtures

	ZrB_2		ZrB_2–SiC	
Processing temperature (°C)	Crystallite size (nm)	Relative density (%)	Crystallite size (nm)	Relative density (%)
600	10	36	10	37
1000	50	35	50	37
1450	600	34	300	40
1650	1000	40	500	95

IV. Densification

The need for dense diboride ceramics was initially driven by nuclear applications that required high neutron absorption cross sections. Later, research was driven by aerospace applications.[71] Without sintering additives, full density has, historically, only been achieved by HP. From the early 1950s to the 1970s, considerable effort was directed at densification of commercially available, non-reactive diboride powders. Research focused on ways to activate sintering so that larger components with more complex shapes could be produced as HP has limits related to both size and geometry. Metallic additives and liquid-phase sintering aids were used to enhance densification. Recent studies have again focused on additives that promote densification, along with some modern densification techniques. As a result, progress has been made in understanding the sintering of diborides while minimizing second phases that may be detrimental to their high-temperature properties. Reports of fully dense diborides, produced by reactive HP date back to 1951,[70] indicating the viability of this approach as well.

This section discusses four densification methods: (1) HP; (2) pressureless sintering; (3) reactive routes; and (4) spark plasma

Table VI. Hot Pressing Conditions and Densities of Hot-Pressed ZrB_2 and HfB_2

Boride	Particle size (μm)	Hot pressing conditions			Final density (%)	References
		Temperature (°C)	Pressure (MPa)	Time (min)		
Historic studies						
ZrB_2	7	2100	~28	80	~95	Chown[99]
$ZrB_{1.89}$	—	1800	~827	—	≤100	Kalish *et al.*[100]
ZrB_2	—	2000	~17	260	99.2	Fenter[101]
ZrB_2	—	2200–2300	29–39	20–30	~95±2	Andrievskii *et al.*[102]
HfB_2	5	1840	~793	10	≤100	Kalish and Clougherty[103]
HfB_2	5	1790	~1,551	10	≤100	Kalish and Clougherty[103]
$HfB_{1.82}$	5	1800	~827	—	≤100	Kalish *et al.*[100]
HfB_2	—	2200	~23	200	98.0	Fenter[101]
Recent studies						
ZrB_2	6	1900	30	30	86.5	Bellosi and colleagues[104,105]
ZrB_2	<2	1900	32	45	99.8	Cutler[9]
HfB_2	~10*	2160	~27	180	90–95	Opeka *et al.*[12]

[—], information not disclosed in the reference. *−325 mesh (nominally ~10 μm on average) HfB_2 powder from Cerac Inc., Milwaukee, WI.

sintering. Induction zone melting has also been used to densify ZrB_2 and HfB_2.[55,97] However, this process was not reviewed because the specimen size (~0.25–0.6 cm) only allowed for limited microstructural analysis (grain size of ~300 μm) and property measurements (microhardness).

(1) HP

Because of strong covalent bonding and low self-diffusion, high temperatures and external pressures are required to densify diborides.[2] Results of early HP studies on commercially available ZrB_2 and HfB_2 powders are summarized in Table VI,[7,12,98–104] which includes details of the starting materials, HP conditions, and final densities. Most of the diborides were presumed to be stoichiometric (B:M = 2.0). However, Kalish *et al.*[99] studied boron-deficient compositions (e.g., $ZrB_{1.98}$ and $Hf_{1.82}$). The $ZrB_{1.98}$ composition was nominally in the single-phase ZrB_2 field and, thus, should not have affected the HP conditions or the resulting microstructure. Metal additions used to produce $HfB_{1.82}$ should place the composition in the HfB_2–HfB two-phase field. It is not clear how this change in composition may have affected densification and the resulting microstructure, but the HP temperature (1800°C) was well below the solidus temperature for the HfB_2–HfB binary (~2100°C). Because no liquid should form, densification would still have to proceed by a diffusion-controlled (as opposed to a liquid phase) mechanism and would be expected to occur at a temperature similar to the stoichiometric diboride. HP of both $ZrB_{1.98}$ and $HfB_{1.82}$ at 1800°C required the application of a high pressure (~827 MPa) to reach full density.

In historic studies, nominally stoichiometric ZrB_2 and HfB_2, without additives, have only been densified by HP at 2000°C or higher with pressures of 20–30 MPa,[105] or at reduced temperatures (1790–1840°C) with much higher pressures (800–1500 MPa).[99,102] Recent studies (also included in Table VI) have produced similar results. Nearly phase pure ZrB_2 and HfB_2, with average starting particle sizes of 5–10 μm, require HP above 2000°C to achieve full density.[104] For example, HfB_2 with a nominal starting particle size of 10 μm was <95% dense after HP at 2160°C and 27.3 MPa for 180 min.[12]

Recent research at UMR showed that commercial ZrB_2 with a ~2 μm starting particle size (Grade B, H. C. Starck, Newton, MA, >99% purity with 0.89% O) can be further comminuted by standard techniques (e.g., attrition milling) to enhance densification. Particle size reduction reduced the HP temperature necessary to achieve full density to 1900°C (pressed for 45 min at 32 MPa).[7] Analysis revealed no porosity, but ~1.9 vol% WC was present. The WC was incorporated during attrition milling due to wear of the WC-based milling media. The microstructure contained both equiaxed and slightly elongated ZrB_2 grains with an average grain size of ~6 μm. Minimization of grain growth was attributed to lower HP temperatures and reduced starting particle sizes. This result can be contrasted with 10–20 μm average grain sizes that are common in diborides processed from coarser ZrB_2 and HfB_2 powders with higher HP temperatures.[12,100,101,106]

Research in the late 1960s on metal (Zr, Hf, Cr, Y, and Al) and ceramic (SiC, $MoSi_2$, and TaB_2) additions to ZrB_2 and HfB_2 revealed the superior densification, and more importantly the improved oxidation and thermal stress resistance (TSR), of diborides containing SiC, C, or SiC plus C.[107,108] Fenter[100] reviewed many compositions, the most important of which were ZrB_2 and HfB_2 with 20 vol% SiC or 18 vol% SiC and 10 vol% C. Subsequent to these key studies, recent research using commercial ZrB_2 and HfB_2 powders has typically included non-reactive additives (e.g., SiC) or liquid phase forming additions (e.g., Ni, Si_3N_4, or $MoSi_2$) to improve densification. The high HP temperatures and pressures of historic studies[99,102] are not necessary with the finer starting powders and additives that minimize grain growth, produce a liquid phase, or result in solid solution formation. In recent studies, both ZrB_2 and HfB_2 have been hot pressed to near full density by adding Ni,[109,110] Si_3N_4,[110,111] AlN,[110,112] $MoSi_2$,[113–115] SiC,[7,116–118] Ta_5Si_3,[119] and other UHTCs, or combinations of additives.[109,120–123] Many of these additives reduced the densification temperature of ZrB_2, with Ni reducing it to as low as 1600°C.[120] However, even with these additions, pressures of 20–50 MPa were required.

(2) Pressureless Sintering (PS)

PS of diborides would enable the fabrication of components to near-net shape using standard powder processing methods. Compared with HP, sintering is more efficient and reduces costs, potentially opening the door for other applications. The two approaches typically used to enhance densification are reduction of starting particle size and the use of sintering aids. Potential sintering aids can be classified into categories including liquid phase formers, solid solution formers, and reactive agents.

Some discrepancy exists for the onset temperature for densification of diborides. Temperatures as low as 1300°–1500°C were reported in historic studies,[98,102] while more realistic temperatures of ~1750°C have been reported recently.[106] The discrepancy is likely due to the purity of the powders. Densification of pure diborides is due to grain boundary and volume diffusion, which are not appreciable until 1800°C or higher.[2] The presence of oxide or metallic impurities increases the driving force for densification, but also enhances grain and pore growth,

which limit the maximum achievable density to 95% or less. In particular, B_2O_3 enhances grain growth and inhibits densification by promoting coarsening at temperatures below 1800°C.[124,125]

Historic studies implied that phase-pure diborides could not be pressurelessly sintered to full density since the hexagonal crystal structure allowed for anisotropic grain growth and entrapped porosity (i.e., coarsening was more favorable than densification). However, Baumgartner and Steiger[126] successfully sintered TiB_2 to >99% density at 2000°–2100°C using submicrometer starting powders. While fine particle size enhanced densification, Baik and Becher[3] later showed that the other key to pressureless densification of TiB_2 was the total oxygen content. Reducing the oxygen content to ≤0.5 wt% minimized evaporation–condensation, which allowed densification to proceed without significant grain or pore growth.

Historic studies on PS of ZrB_2 and HfB_2 are limited, and many were carried out nearly 40 years ago.[127] However, increased densification rates were demonstrated through additions of transition and refractory metals.[127] Meerson and Gorbunov[128] used 0.7 wt% C, along with ZrO_2 and B, to produce nearly fully dense ZrB_2. They hypothesized that the C reduced ZrO_2, which subsequently reacted with the B to produce active ZrB_2 nuclei on the surface of larger ZrB_2 grains. Cech *et al.*[129] added metals to accelerate densification. They reported ~100% density for ZrB_2 sintered at 2200°C for 1 h in argon when adding 1 wt% Re, or 0.5 wt% Cr +0.5 wt% Ti. Lattice parameter measurements after sintering showed metal atom substitution onto Zr sites in the ZrB_2 lattice. They hypothesized that the local contraction of the lattice affected the surface and volume free energies, effectively increasing the driving force for sintering. Coble and Hobbs[124] showed similar results for TiB_2. Kisliy *et al.*[130] used W additions to ZrB_2. They reported significant densification, along with evidence for substitution of some W into the ZrB_2 lattice.

Gropyanov[131] also noted that intensive mechanical milling, vibratory milling in this case, enhanced densification of ZrB_2. He hypothesized that the milling not only increased the surface area, but also increased the number of point defects near the surface of the particles, enhancing the driving force for densification by grain boundary diffusion.

In a recent study of pressureless sintering, Kida and Segawa[132,133] sintered ZrB_2 to 95% relative density without external pressure. However, densification was only possible with significant amounts of BN (5 wt%), AlN (15 wt%), and SiC (5 wt%). Quabdesselam and Munir[134] found that fine TiB_2 produced by SHS did not have improved densification compared with powders produced by carbothermal reduction. Their results demonstrated that powder processing alone does not activate densification. Mishra *et al.*[88] sintered ZrB_2 with a nominal particle size of 2.8 μm, produced by SHS, to a density of 94% at 1800°C for 1 h in flowing argon. They noted a small amount of ZrO_2 during microstructural analysis, but concluded that Fe and Cr impurities promoted local melting, which improved densification. In a subsequent study, Mishra *et al.*[93] focused on Fe and Cr additions to ZrB_2. Although Cr resulted in swelling and cracking, the addition of up to 10 wt% Fe improved density to ~93% at 1800°C. While transition metal additives reduce the densification temperatures for diborides, they also cause marked reductions in melting temperature, hardness, and high-temperature strength.[109,128,129]

Modern ZrB_2 can be sintered to near full density without metal additions. Sciti *et al.*[135] sintered ZrB_2 (Grade B, H. C. Starck, Germany) to full density at 1850°C by adding 20 vol% $MoSi_2$, which led to liquid phase formation. Research at UMR has shown that the same ZrB_2 can be densified using reactive additives.[77,136] With small amounts of WC (~2 vol%), ZrB_2 was sintered to >98% density at 2150°C for 540 min. Analysis by XRD indicated that W and C were incorporated into the ZrB_2 lattice after reaction. Similar to the work of Baik and Becher[3] in TiB_2, densification of ZrB_2 was activated when the oxide impurities (B_2O_3 and ZrO_2) were removed from particle surfaces, which minimized coarsening. Thermodynamic predictions followed by XRD analysis confirmed that ZrO_2 could be removed with either WC or B_4C. However, B_4C reacted with ZrO_2 at lower temperatures (~1200°C) than WC (~1850°C), which reduced the densification temperature (Fig. 3). The microstructures of ZrB_2 sintered with B_4C (Fig. 4) confirm that

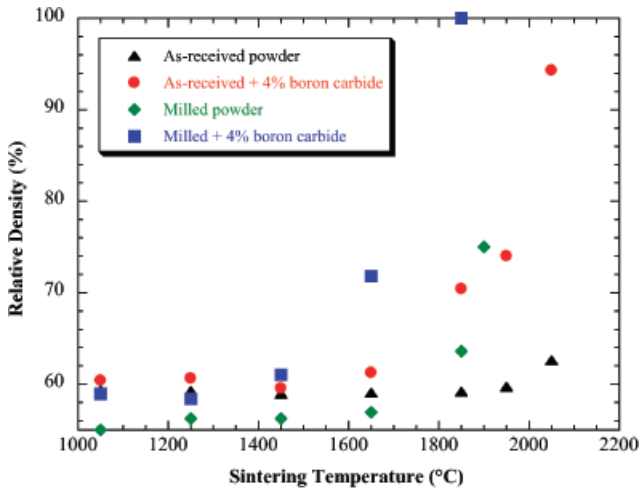

Fig. 3. Relative density as a function of sintering temperature for ZrB_2 (as-received and attrition-milled powders), with and without 4 wt% B_4C additions. The addition of B_4C led to higher relative densities at all sintering temperatures for both attrition-milled powder, achieving 100% of the theoretical density for milled ZrB_2 with 4 wt% B_4C sintered at 1850°C.

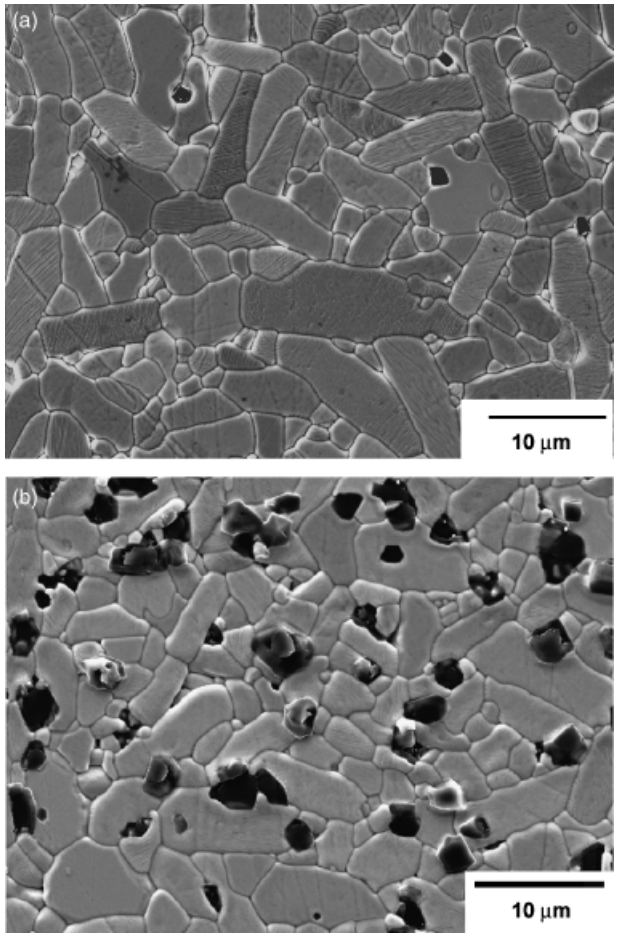

Fig. 4. Microstructure of ZrB_2 sintered at 1850°C for 1 h in vacuum. Specimens were prepared from attrition-milled powder with (a) 2 wt% B_4C and (b) 4 wt% B_4C additions.

dense ceramics can be prepared at temperatures as low as 1850°C.

(3) Reactive Routes to Densification

Synthesis and densification can be combined into single-step, *in situ* reaction and densification processes. Either elemental reactions (Reactions (8) and (9)) or reduction processes (Reactions (1)–(5)) can be used to form diborides by reactive HP (RHP). An extremely fine crystallite size (~10 nm) was achieved for ZrB_2 by reacting Zr and B that were attrition milled.[94] The fine crystallite size should enhance the driving force for sintering, as densification is driven by minimization of surface free energy. However, HP at 2100°C was required to achieve a relative density of 99% for ZrB_2, despite its extremely fine crystallite size, possibly due to grain coarsening below the final densification temperature.[94] For comparison, ZrB_2 ceramics produced from commercially available powders with submicrometer-sized particles could be hot pressed to >99% density at 1900°C.[137] Analysis of scanning electron microscopy (SEM) images revealed an average grain size of ~12 μm for ZrB_2 produced by RHP at 2100°C, compared with ~6 μm for ZrB_2 produced by conventional HP at 1900°C.[137] The crystallite size and density data in Table V confirm significant coarsening in the RHP material. As has been reported for other non-oxide ceramics such as TiB_2,[3] B_4C,[138] and SiC,[139] oxygen impurities in ZrB_2 inhibited densification by promoting coarsening at temperatures below which densification could occur.

Combined *in situ* synthesis and densification processes have also been developed for ZrB_2–SiC[94,140] and HfB_2–SiC.[141] These processes employ reactions of elemental precursors (Zr, B, and SiC)[142] as well as more complex displacement reactions[140,141,143,144]:

$$2Zr + Si + B_4C \rightarrow 2ZrB_2 + SiC \quad (10)$$

$$(2+x)Hf + (1-x)Si + B_4C \rightarrow 2HfB_2 + (1-x)SiC + xHfC \quad (11)$$

The presence of SiC had a dramatic effect on both the densification temperature and the resulting microstructure. Using Zr, B, and SiC as precursors, a relative density of ~95% was achieved by RHP at 1650°C (Table V). Not only was the densification temperature (1650°C) reduced significantly compared with ZrB_2 produced by RHP (2100°C) or conventional HP (1900°C), but the ZrB_2 grain size was also much smaller. Analysis of the microstructure (Fig. 5) revealed an average grain size of ~0.5 μm for ZrB_2–SiC produced by RHP compared with ~12 μm for dense RHP ZrB_2. The reduction in processing temperature for ZrB_2–SiC by RHP has two likely causes: (1) minimization of oxide impurities (B_2O_3, ZrO_2) and (2) fine crystallite/particle sizes.

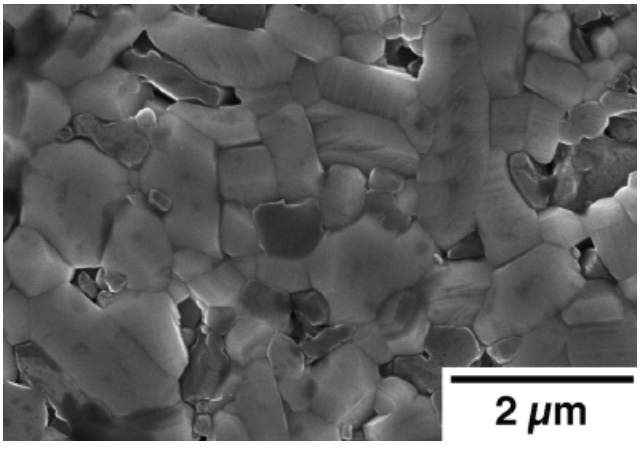

Fig. 5. A polished, thermally etched cross section of a ZrB_2–SiC ceramic prepared by the reactive hot pressing of Zr, B, and SiC at 1650°C. SiC is the darker phase.

(4) Spark Plasma Sintering (SPS)

SPS has recently been applied to densify UHTCs[114,115,122] and other ceramics.[145–147] The SPS process consists of simultaneously applying a uniaxial load and a direct or pulsed electric current to a powder compact. SPS is similar to HP. However, in place of indirect heating, the applied electrical field heats the die and the powder compact (if the powder is electrically conductive). Rapid heating rates (hundreds of °C/min) facilitate rapid densification, which minimizes grain growth. As an example, Monteverde *et al.*[148] used SPS to achieve full density for HfB_2+30 vol% SiC by heating at 100°C/min to 2100°C with a 2 min hold and at 30 MPa. The entire SPS cycle took ~30 min, including heating and cooling, which resulted in a uniform microstructure with a mean grain size of ~2 μm.

Medri *et al.*[122] compared ZrB_2 containing 30 vol% ZrC and 10 vol% SiC prepared by HP and SPS. Despite the addition of 3.7 vol% Si_3N_4 as a sintering aid, the HP specimen had a maximum densification rate of only 1.3×10^{-5} s^{-1} at 1870°C, ultimately reaching only ~90% density. In contrast, the SPS specimen had a nearly constant densification rate of 2×10^{-4} s^{-1} over a broad temperature range (1750°–2050°C), resulting in near full density at 2100°C in <60 min. Similar results were also observed in HP versus SPS comparison studies for HfB_2+15 vol% $MoSi_2$,[114] ZrB_2+15 vol% $MoSi_2$,[115] and HfB_2+30 vol% SiC+2 vol% $TaSi_2$.[149]

V. Microstructure and Mechanical Properties

Besides melting temperature, the properties that make ZrB_2 and HfB_2 attractive for high-temperature structural applications are strength at elevated temperatures and TSR. This section focuses on ZrB_2 and HfB_2, as well as diborides with SiC or $MoSi_2$ additions, from recent studies. The subsections that follow discuss the strength, modulus, hardness, toughness, and TSR of diborides from recent studies.

Results from historic studies are not discussed in this section because the large starting particle size of the powders, higher impurity levels (>0.25 wt% C or Fe), or densification temperatures (>2000°C), which resulted in exaggerated grain growth.[2] Large grains reduced mechanical strength, due, in part, to residual thermal stresses that result from thermal expansion anisotropy.[150] For anisotropic materials, a critical grain size exists below which microcracking can be avoided.[151] While values have not been established for ZrB_2 or HfB_2, the values should be similar to the critical grain size for TiB_2, which is ~15 μm.[152] Hence, microcracking may influence the observed properties of large grained (i.e., >15 μm) diborides. In addition, many studies used additives such as transition metals that reduce strength at elevated temperature ($\sigma_{1000} < 0.3\sigma_{RT}$).[103,104,109,110]

(1) Strength of Diborides

Like most ceramics, higher strengths are reported for diborides with finer grain sizes.[7,114,121,153] The dependence of flexure strength on grain size (Fig. 6) demonstrates that strength increases as grain size decreases for ZrB_2 and HfB_2 based ceramics, with and without $MoSi_2$ or SiC.[7,11,99–101,113–116,118,121,135,140,141,148,154] As indicated in the legend, the plot includes diborides produced by HP, RHP, SPS, and PS. Most strengths were measured in four-point bending, but some authors used three-point bending. Further, specimen size varied, mostly between U.S. and European standards, and, thus, the strengths are not directly comparable. However, strengths, in general, show an inverse square root relation with grain size ($GS^{-1/2}$) as would be expected for ceramics free from other, larger flaws. A line in Fig. 7 is intended to highlight an approximate $GS^{-1/2}$ relationship, not as a fit to the data.

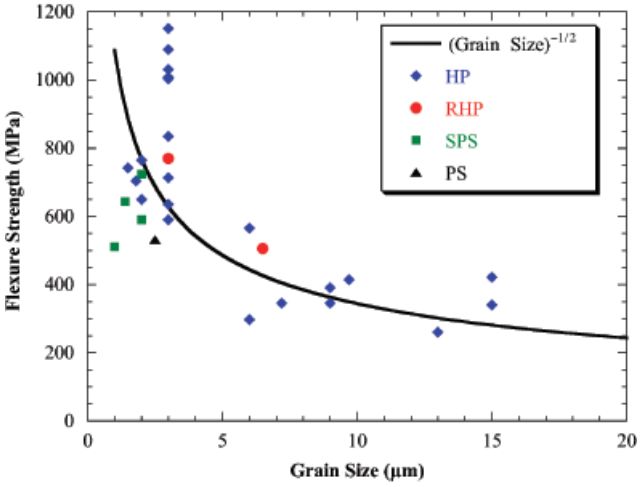

Fig. 6. Room temperature flexure strength as a function of grain size from the diboride literature.

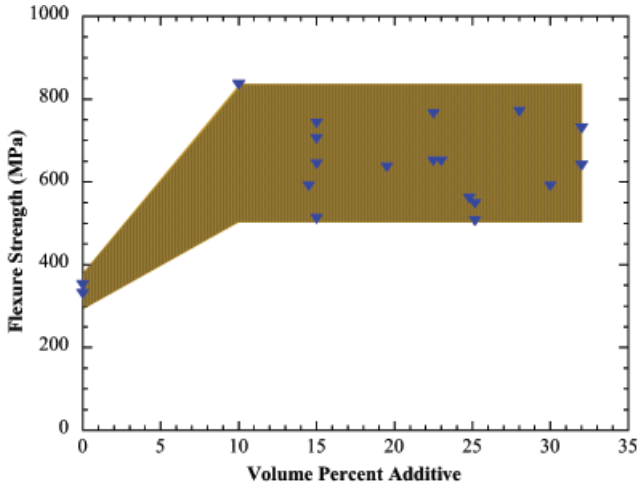

Fig. 8. Room temperature flexure strength as a function of the volume percent additive (e.g., SiC, $MoSi_2$, plus others). The shaded area is intended to indicate that all levels of additives increase the mechanical strength, but that roughly 10 vol% may be enough to maximize strength.

Fabrication of diborides with fine grain size and high strength requires processing below 2000°C (e.g., HP, RHP) or limited time at higher temperatures (e.g., SPS). Second phases such as SiC, $MoSi_2$, ZrC, or HfN that improve densification may also inhibit grain growth and improve strength.[2,100,113,121] Research at UMR has shown that hot-pressed ZrB_2 (no additive) has a strength of 565 MPa (Fig. 7).[7] The addition of 10, 20, or 30 vol% SiC or $MoSi_2$ reduced the average grain size to ~2–3 μm, which increased strength to 700–1000 MPa.[7,113] Considering that the ZrB_2+10 vol% SiC composition was only ~93.2% dense while the other compositions were fully dense,[7] the results indicate that 10 vol% of a second phase may be enough to limit grain growth and maximize strength at room temperature. Room temperature strengths for diborides produced by HP, SPS, and RHP support this conclusion (Fig. 8), particularly the work of Monteverde.[100,103,114,115,117,118,121,123,124,141,148,149,155]

Although ZrB_2 grain size is a factor, the room temperature strength of fine-grained ZrB_2–SiC is not controlled by the size of the ZrB_2 grains.[153,156] Rezaie *et al.*[153] used linear elastic fracture mechanics (Griffith criteria) to show that the critical flaw size correlates strongly to the SiC particle size in ZrB_2–30 vol% SiC ceramics. This conclusion is consistent with analysis of the CTE mismatch between SiC ($\alpha_{avg.}$ ~4×10^{-6} K^{-1}) and HfB_2 ($\alpha_{avg.}$ ~8×10^{-6} K^{-1}) that results in GPa-level residual stresses that may produce microcracks at HfB_2–SiC interfaces.[141] The CTEs of ZrB_2 single crystals were reported to be 6.9×10^{-6} K^{-1} along the *c*-axis and 6.7×10^{-6} K^{-1} along the *a*-axis.[150] The difference in CTE values between the two axes within the hexagonal crystal structure results in a ~95 MPa thermal stress within polycrystalline ZrB_2 when cooled from a typical processing temperature (1900°C).[157] The addition of α-SiC (6H) particles results in larger thermal stresses in ZrB_2–SiC than in polycrystalline ZrB_2 due to the lower CTE of SiC (4.7×10^{-6} and 4.3×10^{-6} K^{-1} along the *c*- and *a*-axis, respectively).[158] An Eshelby analysis (Eq. (12)) of ZrB_2 containing SiC-particulates, assuming spherical SiC inclusions, predicts radial compressive stresses within the ZrB_2 matrix to be as high as 2.1 GPa and tangential tensile stresses of 4.2 GPa at ZrB_2–SiC interfaces[159]:

$$\sigma_{radial} = -2 \times \sigma_{tan} = \frac{(\alpha_m - \alpha_i)\Delta T}{(1-2\nu_i)\,E_i + (1-\nu_m)(2E_m)} \left(\frac{R}{r+R}\right)^3 \quad (12)$$

where m denotes the matrix, i denotes the inclusion, α is the CTE, ν is Poisson's ratio and *E* is Young's modulus. The stresses decrease as distance from the inclusion (*r*) increases, and increase as the inclusion size (*R*) increases.

Based on this analysis, smaller SiC particles reduce the tendency for microcracking and the nucleation of larger, critical flaws.[151] This conclusion is also supported by the strong correlation between the room temperature flexure strength of ZrB_2–30 vol% SiC ceramics and the average SiC grain size, whereas strength does not correlate to average ZrB_2 grain size (Fig. 9). The data for Fig. 9 were obtained from specimens hot pressed at various temperatures and times using a single SiC starting particle size,[153] and from specimens hot pressed using SiC with different particles sizes at the same HP temperature.[156] Analysis of the critical flaw size along with maximum ZrB_2 and SiC grain sizes, confirmed that the maximum SiC grain size in ZrB_2–SiC ceramics is the strength limiting factor.[156]

Second phase additions reduce densification temperature and grain size, but the resulting ceramics may experience mechanical degradation at elevated temperature.[117] Modern, hot-pressed diboride-based composites show a significant loss of strength below 1500°C ($\sigma_{1500} < 0.5\sigma_{RT}$),[115,118,121,123,141] which is well below temperatures expected in proposed applications (>2000°C). Typically, oxide impurities form grain boundary phases or become localized at triple grain junctions, which reduce strength.[121]

In contrast, SPS has been used to produce HfB_2–SiC and HfB_2–$MoSi_2$ ceramics that maintain their room temperature

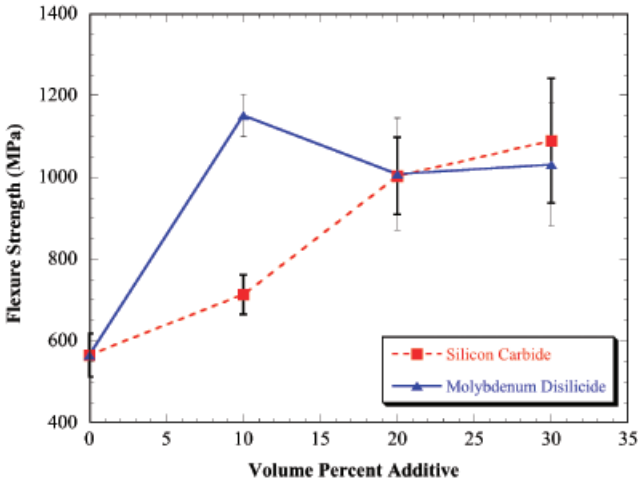

Fig. 7. Room temperature flexure strength as a function of volume percent SiC and $MoSi_2$ in zirconium diboride -based ceramics produced by hot pressing at 1900°C.[7,14]

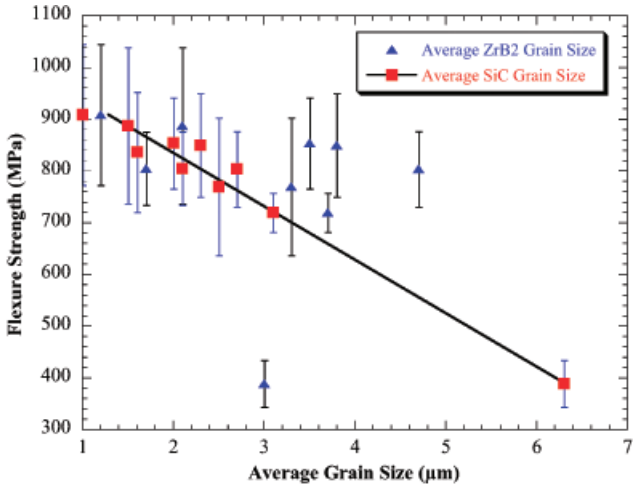

Fig. 9. Room temperature flexure strength as a function of the average zirconium diboride (ZrB_2) grain and SiC particulate size in ZrB_2–30 vol% SiC ceramics (data obtained from Rezaie *et al.*[153] and Zhu *et al.*[156]). The linear curve fit indicates a strong correlation between strength and the size of the SiC particulates.

flexure strength up to 1500°C.[114,115,148] The electrical discharge used to heat the specimen may promote breakdown of the nonconductive oxides on the surface of the particles, perhaps removing them before sintering,[160] which could explain the improved high-temperature mechanical performance reported in recent SPS studies. The HfB_2-based ceramics produced by SPS appear to contain fewer oxide impurities (Si–Hf–C–O) than had been found in ceramics produced from the same powders using conventional HP.[115,148]

Figure 10 is a plot of strength as a function of test temperature for HfB_2–SiC produced in historic studies,[100] and three recent HfB_2-based ceramics produced by HP,[149] RHP,[141] and SPS.[115] Strengths were obtained in four-point bending on similar-sized test bars (~4.9–5 mm^2 in cross-sectional area). However, more strength testing is needed at elevated temperatures. Reporting strength at two temperatures does not provide compelling evidence for the effect of temperature (the dashed lines in Fig. 10 are only included to show general trends). Second, SPS

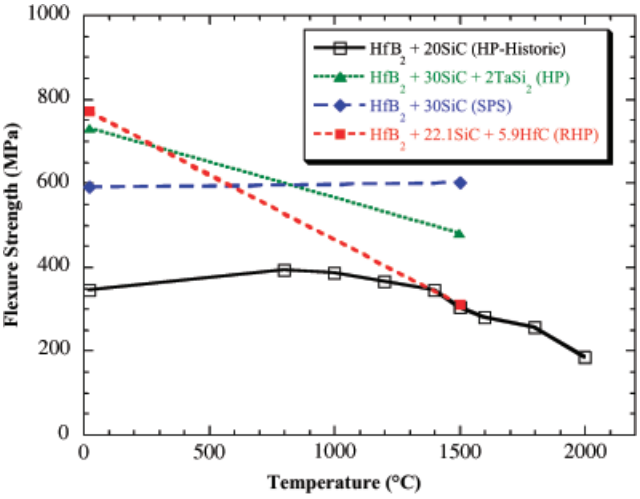

Fig. 10. Flexure strength as a function of test temperature for hafnium diboride (HfB_2) containing 20 vol% SiC produced in the 1960s ([100]) and three recent HfB_2-based ceramics with 22.1–30 vol% SiC additions produced by hot pressing (HP) (Monteverde[149]), RHP (Monteverde[141]), and SPS (Bellosi *et al.*[115]). The dashed lines for the recent HP, reactive HP , and Spark plasma sintering studies are only meant to draw the eye to the suggested trend in the data.

appears to produce materials with superior strengths at elevated temperature ($\sigma_{1500°C}$ is equivalent to σ_{RT}), which merits further investigation. To utilize these materials in the proposed applications, the mechanical response must be understood for temperatures from 1500° to 2500°C (or higher).

(2) Elastic Modulus, Hardness, and Toughness

Room temperature elastic modulus (E), Vickers hardness (H_V), and fracture toughness values for ZrB_2 and HfB_2, pure or with SiC or $MoSi_2$ additions, are summarized in Table VII. Elastic modulus for ZrB_2 (~489 GPa)[7] from recent studies is consistent with values from historic studies using similar sonic resonance techniques on polycrystalline samples.[161] Elastic modulus values for HfB_2 range from 480 to 510 GPa,[8,162] although a value of ~445 GPa was reported for porous HfB_2.[12] Information on elastic constants as a function of temperature has been reported.[162] In general, elastic moduli of diboride composites scales with the volume fraction of additive ($E_{SiC} \sim 475$ GPa[162] and $E_{MoSi_2} \sim 440$ GPa[163]).

Hardness shows a similar trend, generally following mixing rules in relation to the amount and type of phases included in the particulate composites. Reported hardness values were 21–23 GPa[2,7] for polycrystalline ZrB_2 and ~28 GPa[9] for HfB_2. Therefore, additions of SiC (H_V ~28 GPa[164]) to ZrB_2 result in a slight increase in hardness,[7] while SiC additions to HfB_2 result in little or no change in hardness.[115] On the other hand, $MoSi_2$ has a low hardness (~9 GPa[165]) and its addition decreases the hardness of either ZrB_2[113] or HfB_2[114]-based ceramics.

The fracture toughness of ZrB_2 and HfB_2, with and without additives, is generally in the range of 3.5–4.5 $MPa \cdot m^{1/2}$. Fracture toughness values (Table VII) have been obtained using a variety of measurement techniques, so direct comparisons are difficult. In a systematic study of the effect of additive content, Chamberlain *et al.*[7] reported that fracture toughness increased from 3.5 $MPa \cdot m^{1/2}$ for pure ZrB_2 to 5.3 $MPa \cdot m^{1/2}$ for ZrB_2 with 30 vol% SiC. Specimens exhibited crack deflection and crack bridging (Fig. 11). The ZrB_2 grains typically failed in a transgranular manner and cracks deflected at or near ZrB_2–SiC interfaces, leaving SiC particles in the wake of the advancing cracks.[153] This result is consistent with the residual stresses predicted at ZrB_2–SiC interfaces due to the mismatch in thermal and mechanical properties between the dispersed SiC particulates and the ZrB_2 matrix (discussed earlier). Further increases in fracture toughness for diboride-based composites will likely require second phase additions with a higher aspect ratio (e.g., SiC platelets or rods/whiskers)[166,167] or the fabrication of laminate-type architectures.[168,169]

(3) Thermal Stress Resistance

The use of diboride-based ceramics in applications such as rocket nozzles and leading edges may be limited by thermal stress resistance (TSR), which is poor for most ceramics. Thermal stresses, which develop due to the rapid heating or cooling, are controlled by the thermal and mechanical properties of the material.[170,171] Although five thermal shock parameters are commonly used to describe TSR (R, R', R'', R''', and R''''),[172] the R parameter (Eq. (13)) is typically used as the worst case scenario where heating or cooling occurs under conditions of infinite heat transfer:

$$R = \Delta T_{max} = \frac{\sigma(1-\nu)}{\alpha E} \text{ (in units of °C)} \quad (13)$$

where ΔT_{max} is the maximum allowable temperature change under instantaneous heating or cooling that will not initiate fracture, σ is the strength, α is the CTE, ν is Poisson's ratio, and E is Young's modulus. The R' and R'' parameters are the product of R and the thermal conductivity (R' in W/m) and thermal diffusivity (R'', in $cm^2 \cdot °C/s$). The R, R', and R'' parameters predict resistance to crack initiation and are maximized by increasing strength and decreasing Young's modulus. The R''' and

Table VII. Room Temperature Elastic Modulus, Hardness, and Fracture Toughness Values for ZrB_2- and HfB_2-Based Ceramics

Composition (vol%)	Modulus (GPa)	Hardness (GPa)	Toughness (MPa-$m^{1/2}$)	Reference
ZrB_2	489–493	21–23	3.5–4.2	2,7,100
ZrB_2+10 SiC	450–507	24	4.1–4.8	7,118
ZrB_2+20 SiC	466–531	24	4.4	7,100
ZrB_2+30 SiC	484	24	5.3	7
ZrB_2+10 $MoSi_2$	516	20.4	4.1	113
ZrB_2+15 $MoSi_2$	479	14.9–16.2	3.3–4.4	115
ZrB_2+20 $MoSi_2$	489–523	16–18.5	2.3–3	113,135
ZrB_2+30 $MoSi_2$	494	17.7	4	113
ZrB_2+15 α-SiC+4.5 ZrN	467	15.6	5	123
ZrB_2+35 HfB_2+10 α-SiC+4.5 ZrN	494	16.7	4.8	123
ZrB_2+37.5 HfB_2+19.5 α-SiC+3HfN	497	22	—	121
HfB_2	445	—	—	12
HfB_2+20 SiC	544	17.25	4.15	116
HfB_2+30 SiC	512	26	3.9	115,148
HfB_2+15 $MoSi_2$	519–530	15.7–20.9	3.77–3.82	114
HfB_2+20 SiC+3HfN	506	22.3	3.8	115
HfB_2+22.1 SiC+5.9 HfC	520	19	—	141
HfB_2+30 SiC+2 $TaSi_2$	489–506	—	3.6–4.65	149

R'''' parameters predict crack propagation resistance and can be increased by increasing Young's modulus and decreasing strength.[173] However, resistance to crack initiation is arguably more important for the applications proposed for diborides because of the high heating rates and steady-state heat fluxes.

In historic studies, R parameters of 60°–120°C were calculated for ZrB_2 and HfB_2 from room temperature up to ~1200°C, while the R' parameters were 2600–4500 W/m.[99] The diborides offered a clear advantage over other structural ceramics available at the time (BeO, Al_2O_3, SiC, ZrC, and MgO), which was due, largely, to their strength at elevated temperatures. The beneficial role of SiC or SiC+C additions was quantified in terms of improved R′ performance, with ZrB_2-based ceramics achieving ~9600 W/m under steady-state heat flux.[100,174]

No subsequent studies have been published that support the potential advantages of diborides or their composites in terms of their TSR, although a recent study at UMR has focused on experimental measurement of R using water quench tests (see Sidebar 1). The results show that modern diborides have R parameters that are three to four times higher than historical values due to increased strength. Even so, the measured ΔT_{max} (~400°C) is well below what may be encountered in proposed applications.

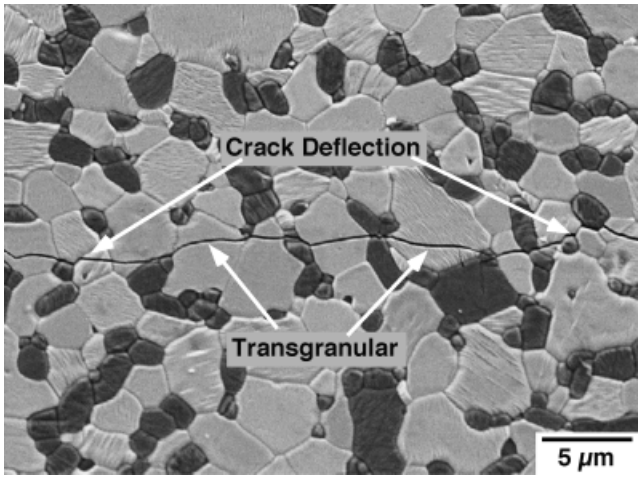

Fig. 11. A thermally etched cross section of zirconium diboride (ZrB_2)–30 vol% SiC hot pressed at 2050°C for 90 min in argon. The image shows a Vickers indentation crack path with inset arrows indicating predominantly transgranular fracture for the ZrB_2 grains and crack deflection near the ZrB_2–SiC interfaces.

One method for improving TSR is to tailor structure on multiple length scales to produce architectures that are engineered to enhance TSR while maintaining load-bearing capability such as fibrous monoliths.[177] Koh measured an R of 1000°C for monolithic Si_3N_4, and 1400°C for a fibrous monolithic ceramic consisting of Si_3N_4 cells and BN cell boundaries. The improved performance was attributed to increased resistance to crack propagation (increased R'''' parameter). Research at UMR on fibrous monoliths with ZrB_2–SiC cells and C–ZrB_2 cell boundaries showed an improvement of ~1000°C in the R parameter compared with conventional materials. However, analysis did not necessarily support the same mechanism for improved performance in ZrB_2-based materials.

VI. Oxidation

Many proposed applications for ZrB_2 and HfB_2 involve oxidizing conditions and elevated temperatures. While other reactive environments (e.g., molten metals, propellants from rocket motors) and erosive conditions are also encountered, this section focuses on static oxidation. The role of additives on oxidation behavior is also discussed. In addition to conventional furnace oxidation and thermal gravimetry (TG) in flowing air, some results from arc heater testing are reviewed.

(1) Pure Diborides

The diborides undergo stoichiometric oxidation when exposed to air at elevated temperatures[178]:

$$ZrB_2(c) + \frac{5}{2}O_2(g) \rightarrow ZrO_2(c) + B_2O_3(l) \quad (14)$$

$$HfB_2(c) + \frac{5}{2}O_2(g) \rightarrow HfO_2(c) + B_2O_3(l) \quad (15)$$

Both reactions are favorable at all temperatures with $\Delta G^{o}_{rxn} = -1977 + 0.361T$ (kJ) for Reaction (14) and $-2003 + 0.374$ (kJ) for Reaction (15). Analysis by TG shows negligible mass gain below ~700°C (Fig. 12). A similar response has been observed for HfB_2, except that its mass gain has been reported to be significantly lower than ZrB_2 at all temperatures.[179] At temperatures below ~1100°C, ZrO_2 (or HfO_2) and B_2O_3

Sidebar 1. Thermal Shock Behavior of ZrB_2-Based Ceramics

A major challenge for ceramics in thermostructural applications is their poor resistance to thermal shock. The primary failure mechanism for pristine monolithic ZrB_2 during thermal shock is crack initiation when the stresses imposed by a thermal gradient exceed the strength of the material. The maximum temperature change (i.e., the R thermal shock parameter) can be calculated using Eq. (S1) and measured properties.

$$R = \frac{\sigma(1-\nu)}{E\,\alpha}\psi \qquad \text{(S1)}$$

where $\boldsymbol{\sigma}$ is the fracture strength, $\boldsymbol{\nu}$ is Poisson's ratio, $\boldsymbol{E}$ is the Young modulus, $\boldsymbol{\alpha}$ is the coefficient of thermal expansion, and $\boldsymbol{\Psi}$ is a stress reduction factor. Based on the properties listed in Table S1, the calculated $\boldsymbol{R}$ parameters for ZrB_2 and ZrB_2–30% SiC were 140° and 200°C, respectively. The values can be compared with a calculated $\boldsymbol{R}$-parameter of ~81°C for monolithic ZrB_2 from historic studies where the fracture strengths were considerably lower (~300 MPa vs. ~823 MPa for the current study). The lower strength of the historic material was due to larger grain sizes from higher HP temperatures.[175]

The experimental thermal shock temperature ($\boldsymbol{R}$) has been determined for ZrB_2 and ZrB_2–30 vol% SiC using water quench thermal shock testing (ASTM C1525) on size B (3 mm × 4 mm × 45 mm) test bars. The thermal shock temperatures for ZrB_2 and ZrB_2–30% SiC were 385° and 395°C (Figure S1). A stress reduction factor ($\boldsymbol{\Psi}$) of 0.36 was required to equate the experimental $\boldsymbol{R}$ for ZrB_2 to the calculated value. If the same $\boldsymbol{\Psi}$ were assumed for ZrB_2–SiC, the "refined" $\boldsymbol{R}$ for ZrB_2–SiC would be 144°C, which is about the same as ZrB_2, compared with a calculated value of 190°C. The discrepancy between the calculated and refined $\boldsymbol{R}$ values for ZrB_2–SiC may be due to microcracking within the particulate composite, which has been reported for a similar diboride material.[176]

In addition to conventional materials, $\boldsymbol{R}$ values were measured for ZrB_2-based fibrous monoliths. As shown in Figure S2, a fibrous monolith was fabricated with cells composed of ZrB_2–30 vol% SiC and cell boundaries composed of graphite–15 vol% ZrB_2. In contrast to the conventional materials, the fibrous monolithic material had an experimental $\boldsymbol{R}$ parameter of ~1400°C (Figure S1), which is ~350% greater than ZrB_2 or ZrB_2–SiC. The strength of the fibrous monolithic material remained constant for $\boldsymbol{T}$ values up to ~1400°C, which represents a marked improvement over the conventional ceramics that lost strength for $\boldsymbol{T}$ values of ~400°C. Previously, Si_3N_4/BN fibrous monoliths have also demonstrated a significant improvement in thermal shock behavior, although the Si_3N_4/BN material had a gradual loss in strength as quench temperature increased that was not observed in the ZrB_2-based fibrous monolith.[177] The improved thermal shock resistance of the ZrB_2-based fibrous monolith compared with conventional ZrB_2 and ZrB_2–SiC has been attributed to the fibrous monolithic structure, which limits the initiation and propagation of cracks to the cell boundaries, allowing the strong cells to remain pristine.

Table S1. Material Properties and Thermal Shock Parameters for ZrB_2 and ZrB_2–30 vol% SiC

Material property	ZrB_2	ZrB_2–30 vol% SiC
Density (g/cm^3)	6.27	5.33
Flexure strength (MPa)	568	823
Young's modulus (GPa)	507	503
Assumed Poisson's ratio	0.16	0.16
Calculated R (°C)	140	200
Experimental R (°C)	~385	~395
Stress reduction factor	0.364 (calculated)	0.364 (assumed)
"Refined" R	140	144

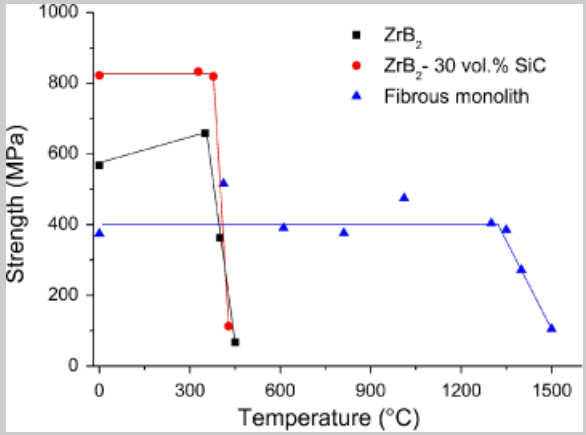

Fig. S1. Flexure strength as a function of change in temperature for water quench thermal testing (ASTM C1525) for ZrB_2, ZrB_2–30 vol% SiC and ZrB_2—30 vol% SiC/graphite—15 vol% ZrB_2 fibrous monoliths.

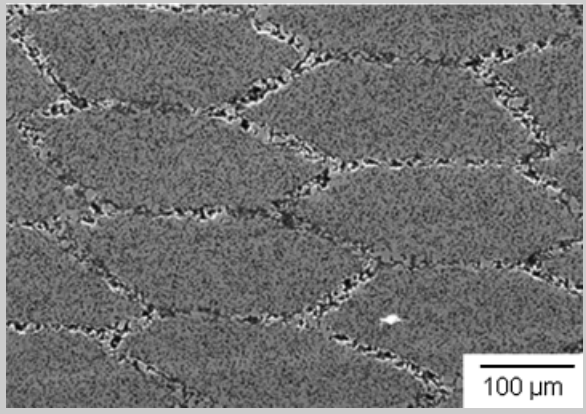

Fig. S2. Scanning electron microscopy image showing the macrostructure of a ZrB_2–SiC/graphite–ZrB_2 fibrous monolith. The architecture consists of ZrB_2–30 vol% SiC cells with a graphite–15 vol% ZrB_2 cell boundary.

form a continuous layer that provides passive oxidation protection.[179–184] Analysis has concluded that the rate limiting step for oxidation is the transport of oxygen through B_2O_3, which results in parabolic (diffusion-limited growth) kinetics for mass gain and the oxide layer thickness, whether the reaction rate was measured by mass gain, oxygen uptake from the atmosphere, or reaction layer thickness.[180,185]

Between ~1100° and ~1400°C, the weight change reflects a combination of mass loss due to B_2O_3 evaporation and mass gain due to the formation of condensed oxides.[182,185] Specimens continue to gain mass as the mass of oxide (ZrO_2 or HfO_2) formed is greater than the mass of diboride reacted plus the mass of B_2O_3 lost. As B_2O_3 evaporates, a porous ZrO_2, layer remains, although a small amount of B_2O_3 may be retained.[143] Above ~1400°C, the oxide layer is not protective and rapid, linear mass gain kinetics have been reported.[180] The TG curve for ZrB_2 in Fig. 12 has an increasing slope, reflecting more rapid mass gain at higher temperatures. In addition to the

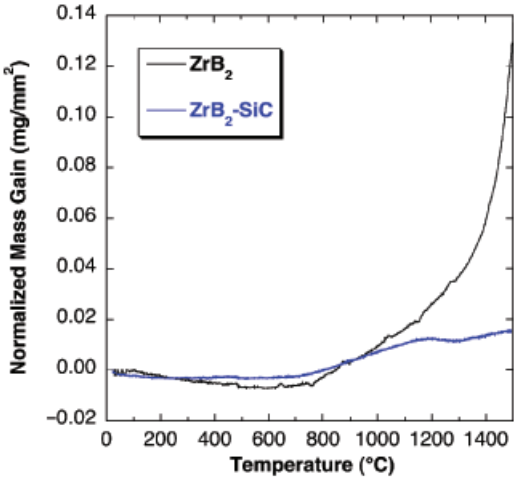

Fig. 12. Weight change measured by thermal gravimetric analysis (TGA) for (a) zirconium diboride (ZrB_2) and (b) ZrB_2 containing 20 vol% SiC heated at 10°C/min to 1500°C in air.

experimental studies, the oxidation behavior of ZrB_2 has been described using various thermodynamic models that focus on oxidation in air at 1500°C or below.[21,186,187]

(2) The Effect of Additives

Additives that alter the composition of the oxide scale improve the oxidation resistance of ZrB_2 and HfB_2. By far, the most common additive is SiC, which reduces the oxidation rate for both ZrB_2 and HfB_2 by forming a silica-rich scale.[177,188–191] Analysis by TG (Fig. 12) shows that ZrB_2–SiC had a normalized mass gain of ~0.02 mg/mm^2 when heated to 1500°C in air compared with a mass gain of ~0.12 mg/mm^2 for ZrB_2. A SiC content of 20 vol% has been studied extensively based on historic studies indicating that this composition had the best combination of oxidation resistance and mechanical behavior.[107] Below ~1100°C, the addition of SiC does not alter the oxidation behavior of the diborides.[182] In this temperature regime, the oxidation rate of SiC is several orders of magnitude slower than that of the diborides.[190] Consequently, the oxide scale on ZrB_2–SiC below 1100°C consists of ZrO_2 and B_2O_3, as it did for pure ZrB_2.[189] Above ~1100°C, two factors affect oxidation. First, the rate of SiC oxidation increases and the SiC particles are converted to SiO_2 plus CO or CO_2. Second, the rate of B_2O_3 evaporation becomes significant. As shown in Fig. 12, ZrB_2–SiC shows a mass loss between 1200° and 1300°C due to B_2O_3 evaporation. The silica-rich layer provides protective behavior, which results in mass gain with parabolic kinetics from room temperature up to at least 1600°C.[21] Analysis of the outer oxide layer formed at 1500°C has detected less than 1 wt% B, indicating that nearly all of the B_2O_3 has evaporated by this temperature.[192] The addition of SiC not only extends the temperature range of protective behavior, but it also imparts the ability to rapidly regain protective behavior after the loss of protection due to excessive temperature, removal of oxide by shear forces, or other causes.

Both ZrB_2–SiC and HfB_2–SiC ceramics exhibit passive oxidation protection with parabolic mass gain kinetics over a wide range of temperatures. The oxidation rate is controlled by diffusion of oxygen through the outer oxide scale. Most authors also report the formation of a layer containing both ZrO_2/HfO_2 and SiO_2 beneath the outer layer. Often, this region is thin compared with the outer silica-rich scale, but thicker layers have been reported after thermal cycling.[153] Below the ZrO_2–SiO_2 (HfO_2–SiO_2) layer, some authors report the formation of a porous region from which SiC has been depleted.[153,190,193–195] This region has been reported to form at temperatures of 1500°C or above and it contains ZrO_2 (HfO_2), ZrB_2 (HfB_2), or both. In dry air, thermodynamic modeling suggested that SiC was removed by active oxidation at the low oxygen partial pressures that are thought to exist under the scale.[196] Subsequent experimental studies confirmed that a porous ZrO_2 layer was formed when ZrB_2–SiC was oxidized at 1500°C in an oxygen partial pressure of ~10^{-10} Pa. Other compounds such as SiC, SiO_2, or B_2O_3 were not detected in the layer.[197]

Besides SiC, additives such as $MoSi_2$,[113,198] tantalum compounds,[119,199] $ZrSi_2$,[195] and other diborides[21,119,200] improve the

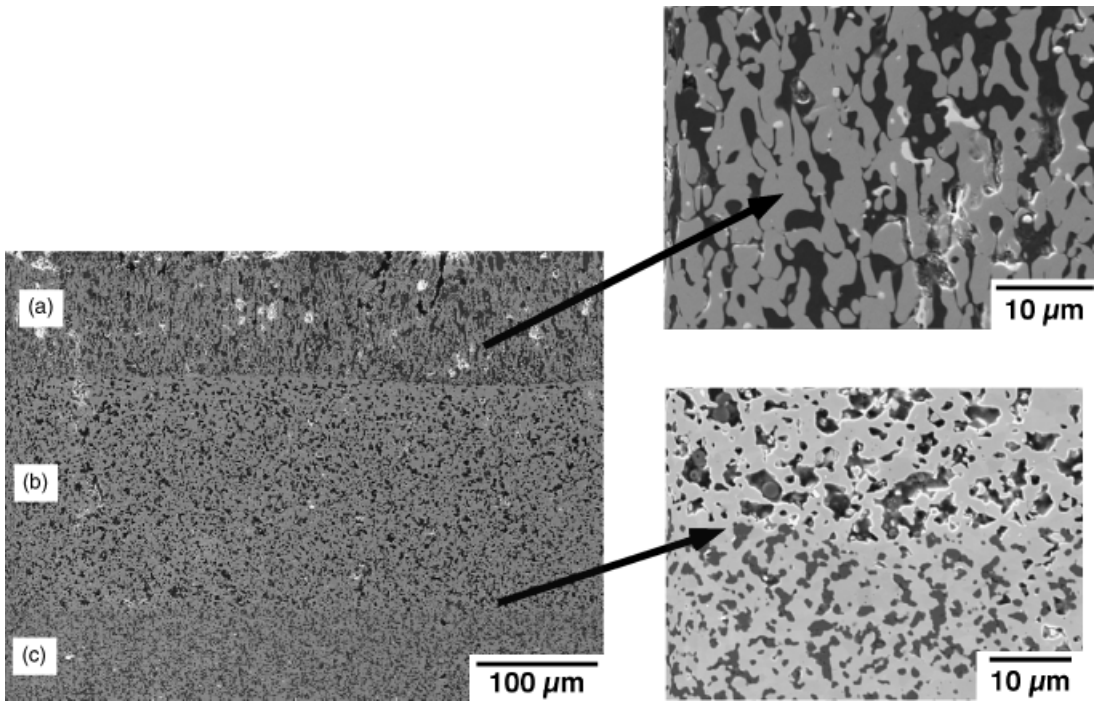

Fig. 13. Cross-sectional scanning electron microscopy image of zirconium diboride (ZrB_2)-SiC after arc heater testing at 350 W/cm^2 showing (a) the mixed oxide layer, (b) the SiC-depleted layer, and (c) the underlying ZrB_2–SiC.

oxidation resistance of diborides either alone or in combination with SiC. In particular, the addition of Ta compounds has been shown to improve the oxidation resistance of ZrB_2–SiC.[119,195,201] These additions alter the composition of the outer glassy layer, which can lead to phase separation of the liquid/glass due to the high cation field strength of the transition metals.[119,201] In the case of Ta additions, the phase-separated glassy layers resulted in reduced oxidation rates in TG studies with ZrB_2–SiC containing TaB_2 having the lowest oxidation rate of any of the materials evaluated.[201]

(3) Arc Heater Testing

Although less common than TG or furnace oxidation studies, arc heater[‡] testing is widely recognized as more representative of the environment that will be encountered in hypersonic flight or atmospheric re-entry because of its high heat fluxes, low pressure dissociated atmosphere (i.e., O instead of O_2), and high gas velocities.[116,196,195,201] Despite the drastic differences in the experimental conditions, the response of boride-based ceramics to arc heater testing appears to be similar to conventional studies. After testing at a heat flux of 350 W/cm^2 for 10 min (surface modified temperature $\sim$1800°C), ZrB_2–SiC formed a surface layer of ZrO_2, a mixed oxide layer, and a SiC-depleted layer (Fig. 13).[196] HfB_2–SiC showed a similar response under the same test conditions.[116] A solid solution modified composition, $(Zr_{0.9},Cr_{0.1})B_2$–SiC, tested by NSWCCD at a heat flux of 326 W/cm^2 showed a reduced erosion rate compared with other materials. For both ZrB_2-SiC and HfB_2–SiC, the dense oxide layer (ZrO_2 or HfO_2) that formed on the surface contained a small volume fraction of holes thought to allow gaseous reaction products (i.e., CO, CO_2, boron and silicon oxides) to escape without disrupting large sections of the scale.[116,196] Based on these arc heater evaluations, ZrB_2–SiC and HfB_2–SiC exhibit protective behavior under a wide range of testing conditions.

VII. Summary

Historic and modern studies of the crystal chemistry, synthesis, densification, microstructure, mechanical properties, and oxidation of ZrB_2 and HfB_2 ceramics were reviewed. Zirconium and hafnium diborides have the AlB_2 structure (*P6/mmm*) that is composed of alternating planes of hexagonally close-packed Zr atoms and graphite-like B atoms. These compounds exhibit partial or complete solubility with other transition metal diborides, which allows properties such as hardness and CTE to be controlled through the application of crystal chemical principles. Commercial diboride powders, with particle sizes as fine as 2 μm, are commonly synthesized by carbothermal reduction. Nano-crystalline powders can be synthesized using solution precursors, exothermic reactions, or pre-ceramic polymers. While HP is the dominant densification technique, recent advances have led to pressureless densification processes through solid-state or liquid-phase sintering. Generally, the strength of the diborides increases as grain size decreases with strengths as high as $\sim$500 MPa reported for materials with grain sizes of $\sim$5 μm. The addition of second phases such as SiC can increase strength to over 1 GPa by further reducing grain size and promoting favorable residual thermal stresses. Further, SPS has been used to produce diboride-based materials that retain their room temperature strength to at least 1500°C. Progress has also been made with regard to understanding the behavior of diboride-based ceramics in static oxidation as well as arc heater testing, which more accurately reproduces environments encountered during hypersonic flight and atmospheric re-entry.

Although significant gains have been made, several critical areas have been identified for future research. In particular, research is needed to understand oxidation mechanisms and fundamental structure-property relations at elevated temperatures, if these materials are to be used in hypersonic, atmospheric re-entry, or rocket propulsion applications.

[‡]A general description of arc heater testing can be found at http://thermo-physics.arc.nasa.gov/arcjet.htm

Acknowledgments

The effort to write this paper was catalyzed by the "NSF-AFOSR Joint Workshop on Future Ultra High Temperature Materials" held at the National Science Foundation in January 2004. Dr. Lynnette Madsen, Ceramics Program Director at NSF, and Dr. Joan Fuller, Program Manager for Ceramics and Non-Metallic Materials at AFOSR, provided the vision for the workshop, which was funded on NSF grant DMR-0403004. G. E. H. and W. G. F. gratefully acknowledge contributions of current and former members of the UMR UHTC research group.

References

[1]A. E. McHale (ed.) *Data Collected from Phase Diagrams for Ceramists*, Vol. X. American Ceramic Society, Westerville, OH, 1994.
[2]R. Telle, L. S. Sigl, and K. Takagi, "Boride-Based Hard Materials"; pp. 802–945 in *Handbook of Ceramic Hard Materials*, Edited by R. Riedel. Wiley-VCH, Weinheim, Germany, 2000.
[3]S. Baik and P. F. Becher, "Effect of Oxygen on the Densification of TiB_2," *J. Am. Ceram. Soc.*, **70** [8] 527–30 (1987).
[4]R. G. Munro, "Material Properties of Titanium Diboride," *J. Res. Natl. Inst. Stand. Technol.*, **105** [5] 709–20 (2000).
[5]Card number 75-1050, Powder Diffraction File, International Centre for Diffraction Data.
[6]Card number 89-3651, Powder Diffraction File, International Centre for Diffraction Data.
[7]A. L. Chamberlain, W. G. Fahrenholtz, G. E. Hilmas, and D. T. Ellerby, "High Strength ZrB_2-Based Ceramics," *J. Am. Ceram. Soc.*, **87** [6] 1170–2 (2004).
[8]P. Vajeeston, P. Ravindran, C. Ravi, and R. Asokamani, "Electronic Structure, Bonding, and Ground State Properties of AlB_2-Type Transition Metal Diborides," *Phys. Rev. B*, **63** [4] 04115–1–11 (2001).
[9]R. A. Cutler, "Engineering Properties of Borides"; pp. 787–803 in *Ceramics and Glasses: Engineered Materials Handbook*, Vol. 4, Edited by S. J. Schneider Jr. ASM International, Materials Park, OH, 1991.
[10]M. W. Jr. Chase, *NIST-JANAF Thermochemical Tables*. American Chemical Society and the American Institute of Physics, Woodbury, NY, 1998.
[11]E. Wuchina, M. Opeka, S. Causey, K. Buesking, J. Spain, A. Cull, J. Routbort, and F. Guitierrez-Mora, "Designing for Ultrahigh-Temperature Applications: The Mechanical and Thermal Properties of HfB_2, HfC_x, and α-Hf(N)," *J. Mater. Sci.*, **39** [19] 5939–49 (2004).
[12]M. M. Opeka, I. G. Talmy, E. J. Wuchina, J. A. Zaykoski, and S. J. Causey, "Mechanical, Thermal, and Oxidation Properties of Hafnium and Zirconium Compounds," *J. Eur. Ceram. Soc.*, **19** [13–14] 2405–14 (1999).
[13]K. Kuwabara, S. Sakamoto, O. Kida, T. Ishino, T. Kodama, H. Nakajima, T. Ito, and Y. Hirakawa, "Corrosion Resistance and Electrical Resistivity of ZrB_2 Monolithic Refractories"; pp. 302–5 in *The Proceedings of UNITECR 2003. The 8th Biennial Worldwide Conference on Refractories*, Osaka, Japan. Edited by K. Asano. Technical Association of Refractories, Japan, 2003.
[14]O. Kida, "Monolithic Refractory Material and Waste Melting Furnace Using the Same," Japanese Patent JP2000335969, May 12, 2000.
[15]N. Kaji, H. Shikano, and I. Tanaka, "Development of ZrB_2-Graphite Protective Sleeve for Submerged Nozzle," *Taikabutsu Overseas*, **14** [2] 39–43 (1992).
[16]B. Stucker, W. Bradley, P. T. Eubank, S. Norasetthekul, and B. Bozkurt, "Zirconium Diboride/Copper EDM Electrodes From Selective Laser Sintering," *Solid Freeform Fabric. Symp. Proc.*, **1**, 257–65 (1997).
[17]Z. J. Jin, M. Zhang, D. M. Guo, and R. K. Kang, "Electroforming of Copper/ZrB_2 Composite Coating and Its Performance as Electro-Discharge Machining Electrodes," *Key Eng. Mater.*, **291–292**, 537–42 (2005).
[18]B. Stucker, M. Malhorta, and Z. Qu, "Recent Developments in the Selective Laser Sintering of Zykron EDM Electrodes"; in *Proceedings of the Laser Materials Processing Conference 1999, San Diego, CA. 87(2) F/158-F/161*. Laser Institute of America, 2000.
[19]J. Sung, D. M. Goedde, G. S. Girolami, and J. R. Abelson, "Remote-Plasma Chemical Vapor Deposition of Conformal ZrB_2 Films at Low Temperature: A Promising Diffusion Barrier for Ultralarge Scale Integrated Electronics," *J. Appl. Phys.*, **91** [6] 3904–11 (2002).
[20]Y. Murata, "Cutting Tool Tips and Ceramics Containing Hafnium Nitride and Zirconium Diboride," *U.S. Patent*, **3**, 487–594 (1970).
[21]M. M. Opeka, I. G. Talmy, and J. A. Zaykoski, "Oxidation-Based Materials Selection for 2000°C+ Hypersonic Aerosurfaces: Theoretical Considerations and Historical Experience," *J. Mater. Sci.*, **39** [19] 5887–904 (2004).
[22]D. M. Van Wie, D. G. Jr. Drewry, D. E. King, and C. M. Hudson, "The Hypersonic Environment: Required Operating Conditions and Design Challenges," *J. Mater. Sci.*, **39** [19] 5915–24 (2004).
[23]M. E. White and W. R. Price, "Affordable Hypersonic Missiles for Long-Range Precision Strike," *J. Hopkins APL Tech. Digest*, **20** [3] 415–23 (1999).
[24]T. A. Jackson, D. R. Eklund, and A. J. Fink, "High Speed Propulsion: Performance Advantage of Advanced Materials," *J. Mater. Sci.*, **39** [19] 5905–13 (2004).
[25]G. V. Samsonov, L. Ya. Markovsky, A. F. Zhigach, and M. G. Valyashko, "Boron, Its Compounds and Alloys," *Akad. Nauk Ukrain. SSR. Kiev.*, (1960) (in Russian).
[26]G. V. Samsonov, T. I. Serebryakova, and V. A. Neronov, *Borides*. Atomizdat, Moscow, 1975.

[27]G. V. Samsonov and K. I. Portnoi. "Alloys Based on High-Temperature Compounds" (Splavy na Osnove Tugoplavkikh Soedineniy), Oboronnoi Prom., Moscow, (1961) (English Translation).
[28]G. V. Samsonov and B. A. Kovenskaya, "The Nature of the Chemical Bond in Borides"; pp. 19–30 in *Boron and Refractory Borides*, Edited by V. I. Markovich. Springer-Verlag, Berlin, 1977.
[29]J. L. Hoard and R. E. Hughes, "Elemental Boron and Compounds of High Boron Content: Structure, Properties, and Polymorphism"; pp. 131–41 in *The Chemistry of Boron and Its Compounds*, Edited by E. L. Muetterties. John Wiley&Sons Inc., New York, 1967.
[30]B. Post, F. W. Glaser, and D. Moskowitz, "Transition Metal Diborides," *Acta Metall.*, **2** [1] 20–5 (1954).
[31]Y. B. Kuz'ma and S. I. Mikhalenko, "Crystal Chemistry of Refractory Compounds," *Zh. Vses. Khim. Obshch. Mendeleeva*, **30** [6] 509–14 (1985).
[32]Y. B. Kuz'ma "Crystal Chemistry of Borides" (Kristallokhimia boridov), Vishcha Skola, Lvov, USSR, 1983.
[33]A. L. Ivanovskii, N. E. Medvedeva, G. P. Shveikin, Y. E. Medvedeva, and A. E. Nikiforov, "First Principles Studies of the Stability and Electronic Properties of Metal Borides. 1. Diborides of 3d Metals," *Metall. Nov. Takhnol.*, **20** [11] 41–9 (1998).
[34]A. L. Ivanovskii, N. E. Medvedeva, and Y. Y. Medvedeva, "Ab Initio Studies of the Stability and Electronic Properties of Metal Borides. II. Diborides of 4d and 5d Metals," *Metall. Nov. Tekhnol.*, **21** [12] 19–33 (1999).
[35]I. R. Shein and A. L. Ivanovskii, "The Band Structure of Hexagonal Diborides ZrB_2, VB_2, NbB_2 and TaB_2 in Comparison With Superconducting MgB_2," *Phys. Solid State (Translation of Fizika Tverdogo Tela (Sankt-Peterburg))*, **44** [10] 1833–9 (2002).
[36]R. Kiessling, "Manganese Borides," *Acta Chem. Scand.*, **4**, 146–59 (1950).
[37]G. Haigg and R. Kiessling, "Distribution Equilibria in some Ternary Systems M1–M2–B and the Relative Strength of the Transition Metal–Boron Bonds," *J. Inst. Metals*, **81**, 57–60 (1952).
[38]K. E. Spear, "Chemical Bonding in AlB_2-type Borides," *J. Less-Common Metals*, **47**, 195–201 (1976).
[39]V. Grigorovich, "Sintering From Aspect of Interatomic Bonds," *Sci. Sintering*, **24** [3] 155–60 (1992).
[40]W. N. Lipscomb and D. Britton, "Valence Structure of Higher Borides," *J. Chem. Phys.*, **33**, 275–80 (1960).
[41]I. I. Lyakhovskaya, T. M. Zimkina, and V. A. Fomichev, "*K*-spectra of Boron in Transition Metal Diborides and in Compounds LaB_6, BaB_6, and AsB," *Fyz. Tverd. Tela (Solid State Phys.)*, **12** [1] 174–80 (1970).
[42]S. A. Nemnonov and K. M. Kolobova, "X-Ray Spectra, Electron Structure, and Properties of Titanium Compounds," *Fiz. Metall. Metalloved. (Phys. Metals Sci. Metals)*, **22** [5] 680–92 (1966).
[43]D. W. Fischer and W. L. Baun, "Band Structure and the Titanium L (sub II, III) X-ray Emission and Absorption Spectra from Pure Metal, Oxides, Nitride, Carbide, and Boride," *J. Appl. Phys.*, **39** [10] 4757–76 (1968).
[44]S. A. Nemnonov, A. Z. Menshikov, K. M. Kolobova, E. Z. Kurmayev, and V. A. Trapeznikov, "Study of the Electronic Structure and Interatomic Bonds in Some Compounds and Binary Alloys by the Method of X-Ray Spectroscopy," *Trans. Metall. Soc. AIME*, **245** [6] 1191–8 (1969).
[45]A. H. Silver and P. J. Bray, "NMR Study of Bonding in Some Solid Boron Compounds," *J. Chem. Phys.*, **32** [1] 288–92 (1960).
[46]G. Grimvall and A. F. Guillermet, "Phase Stability Properties of Transition Metal Diborides"; pp. 423–30 in *Boron-Rich Solids, AIP Conference Proceedings*, Vol. 231, Edited by D. Emin, T. L. Aselage, A. C. Switendick, B. Morosin, and C. L. Beckel. American Institute of Physics, New York, 1990.
[47]T. Lundstroem, "Structure, Defects, and Properties of Some Refractory Borides," *Pure Appl. Chem.*, **57** [10] 1383–90 (1985).
[48]E. M. Savitskii, N. I. Timofeeva, and V. I. Bakarinova, "Chemical Stability of Hafnium Diboride," *Izv. Akad. Nauk SSSR Neorganich. Mater.*, **6** [1] 120–1 (1970).
[49]A. A. Ivan'ko, *Handbook of Hardness Data.* Naukova Dumka, Kiev, 1968.
[50]E. V. Clougherty and R. L. Pober, "Physical and Mechanical Properties of Transition Metal Diborides," *IMD Spec. Rep. Ser.*, **10** [13] 423–44 (1964).
[51]R. Kiessling, "The Crystal Structure of Molybdenum and Tungsten Borides," *Acta Chem. Scand.*, **1**, 893–916 (1947).
[52]F. W. Vahldiek, "Electrical Resistivity, Elastic Modulus and Debye Temperature of Titanium Diboride," *J. Less-Common Metal*, **12** [3] 202–9 (1967).
[53]J. J. Gilman and B. W. Roberts, "Elastic Constants of TiC and TiB_2," *J. Appl. Phys.*, **32** [7] 1405 (1961).
[54]G. V. Samsonov and V. S. Neshpor, "Some Physical Properties of Cermets," *Vop. Poroshkovoi Met. I Prochnosti Mater. Akad. Nauk Ukr. SSR*, **5**, 3–34 (1958).
[55]R. D. Koester and D. P. Moak, "Hot Hardness of Selected Borides, Oxides and Carbides to 1900°C," *J. Am. Ceram. Soc.*, **50** [6] 290–6 (1967).
[56]D. C. Gillies and D. Lewis, "Bond Strength in Diborides of Some Group IV and V Metals," *J. Less-Common Metals*, **16** [2] 162–3 (1968).
[57]F. G. Keihn and E. J. Keplin, "High-Temperature Thermal Expansion of Certain Group IV and Group V Diborides," *J. Am. Cer. Soc.*, **50** [2] 81–4 (1967).
[58]G. V. Samsonov, "Thermal Expansion of Diborides of Group IV and V Transition Metals," *Tepl. Vysok. Temp.*, **9** [1] 195–7 (1971).
[59]B. Lönnberg, "Thermal Expansion Studies on the Group IV–VII Transition Metal Diborides," *J. Less-Common Metals*, **141** [1] 145–56 (1988).
[60]C. Mroz, "Processing TiZrC and $TiZrB_2$," *Am. Ceram. Soc. Bull.*, **73** [4] 78–81 (1994).
[61]H. B. Lee, Y. J. Yoon, Y. K. Oh, and Z. S. Ahn, "Study on Synthesis and Characterization of $TiZrB_2$ Composite by Microwave SHS," *J. Kor. Ceram. Soc*, **36** [1] 7–14 (1999).
[62]M. Moriyama, H. Aoki, and Y. Kobayashi, "Fabrication and Mechanical Properties of Hot-Pressed TiB_2–ZrB_2 Ceramic System," *J. Ceram. Soc. Jpn.*, **106** [12] 1196–200 (1998).
[63]G. V. Samsonov and V. S. Neshpor, "Investigation of the Laws of Formation of Isomorphous Boride Alloys," *Zh. Fiz. Khim.*, **29**, 839–45 (1955).
[64]I. G. Talmy, E. J. Wuchina, J. A. Zaykoski, and M. M. Opeka, "Properties of Ceramics in the NbB_2–CrB_2 System," *Ceram. Eng. Sci. Proc.*, **17** [3] 128–35 (1996).
[65]I. G. Talmy, E. J. Wuchina, J. A. Zaykoski, and M. M. Opeka, "Ceramics in the NbB_2–CrB_2 System"; pp. 81–7 in *Ceramic Matrix Composites- Advanced High Temperature Structural Materials, Materials Research Society Symposium Proceedings*, **Vol. 365**, Edited by R. A. Lowden, M. K. Ferber, J. R. Hellmann, K. K. Chawla, and S. P. DiPietro. Materials Research Society, Warrendale, PA, 1995.
[66]G. A. Meerson, G. V. Samsonov, R. B. Kotel'nikov, M. S. Voinova, I. P. Evteeva, and S. D. Krasnenkova, "Certain Properties of Alloys in the Systems TiB_2–CrB, TiB_2–W_2B_5, and ZrB–CrB_2," *Sbornik Nauch. Trudov. Nauch.-Tekh. Obshchestva Tsvetnoi Met. Moskov. Inst. Tsvetn. Metal. i Zolota*, **29**, 323–8 (1959).
[67]M. Shibuya, M. Kawata, M. Ohyanagi, and Z. A. Munir, "Titanium Diboride–Tungsten Diboride Solid Solutions Formed by Induction-Field-Activated Combustion Synthesis," *J. Am. Ceram. Soc.*, **86** [4] 706–10 (2003).
[68]W. A. Zdaniewski, "Solid Solubility Effect on Properties of Titanium Diboride," *J. Am. Ceram. Soc.*, **70** [11] 793–7 (1987).
[69]E. Fendler, O. Babushkin, T. Lindbaeck, R. Telle, and G. Petzow, "Thermal Expansion of Diboride Solid Solutions"; pp. 204–212 in *Proceedings of the 4th International Symposium on Ceramic Materials and Components for Engines, June 10–12, 1991*, Goteborg. Edited by R. Carlsson, T. Johannson, and L. Kahlman. Elsevier Applied Science, London, 1992.
[70]P. Schwarzkopf and R. Kieffer, *Refractory Hard Metals. Chapter 26.* MacMillan Co., New York, 1953.
[71]R. Thomson, "Production, Fabrication, and Uses of Borides"; pp. 113–20 in *The Physics and Chemistry of Carbides, Nitrides and Borides*, Edited by R. Freer. Kluwer Academic Publishers, Dordrecht, 1990.
[72]T. Lundström, "Transition Metal Borides"; pp. 351–76 in *Boron and Refractory Borides*, Edited by V. I. Markovich. Springer-Verlag, Berlin, 1977.
[73]C. Mroz, "Zirconium Diboride," *Am. Ceram. Soc. Bull.*, **73** [6] 141–2 (1994).
[74]C. Mroz, "Processing and Properties of Microcomposite TiZrC and $TiZrB_2$ Materials," *Ceram. Eng. Sci. Proc.*, **14** [9–10] 725–35 (1993).
[75]H. Zhao, Y. He, and Z. Jin, "Preparation of ZrB_2 Powder," *J. Am. Ceram. Soc.*, **78** [9] 2534–6 (1995).
[76]A. Goldstein, Y. Geffen, and A. Goldenberg, "Boron Carbide-Zirconium Diboride *In-Situ* Composites by the Reactive Pressureless Sintering of Boron Carbide-Zirconia Mixtures," *J. Am. Ceram. Soc.*, **84** [3] 642–4 (2001).
[77]S. C. Zhang, G. E. Hilmas, and W. G. Fahrenholtz, "Pressureless Densification of Zirconium Diboride With Boron Carbide Additions," *J. Am. Ceram. Soc.*, **89** [5] 1544–50 (2006).
[78]L. Chen, Y. Gu, L. Shi, Z. Yang, J. Ma, and Y. Qian, "Synthesis and Oxidation of Nanocrystalline HfB_2," *J. Alloys Comp.*, **368** [1–2] 353–6 (2004).
[79]L. Chen, Y. Gu, Z. Yang, L. Shi, J. Ma, and Y. Qian, "Preparation and Some Properties of Nanocrystalline ZrB_2 Powders," *Script. Mater.*, **50** [7] 959–61 (2004).
[80]D. L. Segal, "Chemical Routes for the Preparation of Powders"; pp. 3–11 in *The Physics and Chemistry of Carbides, Nitrides, and Borides*, Edited by R. Freer. Kluwer Academic Press, Dordrecht, 1990.
[81]M. D. Sacks, C.-A. Wang, Z. Yang, and A. Jain, "Carbothermal Reduction Synthesis of Nanocrystalline Zirconium Carbide and Hafnium Carbide Powders Using Solution-Derived Precursors," *J. Mater. Sci.*, **39** [19] 6057–66 (2004).
[82]K. Su and L. G. Sneddon, "A Polymer Precursor Route to Metal Borides," *Chem. Mater.*, **5** [11] 1659–68 (1993).
[83]S. T. Schwab, C. A. Stewart, K. W. Dudeck, S. M. Kozmina, J. D. Katz, B. Bartram, E. J. Wuchina, W. J. Kroenke, and G. Courtin, "Polymeric Precursors to Refractory Diborides," *J. Mater. Sci.*, **39** [19] 6051–5 (2004).
[84]G. A. Zank U.S. Patent 5,449,646 issued September 12, 1995.
[85]X.-J. Zhou, G.-J. Zhang, Y.-G. Li, Y.-M. Kan, and P.-L. Wang, "Hot Pressed ZrB_2–SiC–C Ultra High Temperature Ceramics With Polycarbosilane as a Precursor," *Mater. Lett.*, **61** [4–5] 960–963 (2007).
[86]Y. D. Blum and H.-J. Kleebe, "Chemical Reactivities of Hafnium and Its Derived Boride, Carbide, and Nitride Compounds at Relatively Mild Temperatures," *J. Mater. Sci.*, **39** [19] 6023–42 (2004).
[87]Y. D. Blum, S. Young, and D. Hui, "Chemical Reactivity: In Search of Better Processing of HfB_2/SiC UHTC Composites"; pp. 103–14 in *Ceramic Transactions Vol. 177: Innovative Processing and Synthesis of Ceramics, Glasses and Composites IX*, Edited by J. P. Singh, N. P. Bansal, B. G. Nair, T. Ohji, and A. R. de Arellano Lopez. American Ceramic Society, Westerville, OH, 2005.
[88]S. K. Mishra (Pathak), S. Das, S. K. Das, and P. Ramachandrarao, "Sintering Studies on Ultrafine ZrB_2 Powder Produced by a Self-Propagating High-Temperature Synthesis Process," *J. Mater. Res.*, **15** [11] 2499–504 (2000).
[89]H. J. Feng, J. J. Moore, and D. G. Wirth, "Combustion Synthesis of Ceramic-Metal Composite Materials: The Zirconium Diboride–Alumina–Aluminum System," *Int. J. Self-Propagating High Temp. Synth.*, **1** [2] 228–38 (1992).
[90]D. D. Radev and D. Klissurski, "Mechanochemical Synthesis and SHS of Diborides of Titanium and Zirconium," *J. Mater. Synth. Process.*, **9** [3] 131–6 (2001).
[91]S. K. Mishra, S. Das, and L. C. Pathak, "Defect Structures in Zirconium Diboride Powder Prepared by Self-Propagating High-Temperature Synthesis," *Mater. Sci. Eng. A*, **A364**, 249–55 (2004).
[92]T. Tsuchida and S. Yamamoto, "Mechanical Activation Assisted Self-Propagating High-Temperature Synthesis of ZrC and ZrB_2 in Air from Zr/B/C Powder Mixtures," *J. Eur. Ceram. Soc.*, **24** [1] 45–51 (2004).
[93]S. K. Mishra, S. K. Das, A. K. Ray, and R. Ramachandrarao, "Effect of Fe and Cr Addition on the Sintering Behavior of ZrB_2 Produced by Self-Propagating High-Temperature Synthesis," *J. Am. Ceram. Soc.*, **85** [11] 2846–8 (2002).

[94]A. L. Chamberlain, W. G. Fahrenholtz, and G. E. Hilmas, "Reactive Hot Pressing of Zirconium Diboride," *J. Mater. Res.*, (2006) (submitted to).
[95]S. L. Dole, S. Prochazka, and R. H. Doremus, "Microstructural Coarsening During Sintering of Boron Carbide," *J. Am. Ceram. Soc.*, **72** [6] 958–66 (1989).
[96]H. K. Lee, R. F. Speyer, and W. S. Hackenberger, "Sintering of Boron Carbide Heat-Treated With Hydrogen," *J. Am. Ceram. Soc.*, **85** [8] 2131–3 (2002).
[97]W. A. Sanders and H. B. Probst, "Hardness of Five Borides at 1625°C," *J. Am. Ceram. Soc.*, **49** [4] 231–2 (1966).
[98]J. Chown, "The Hot Pressing of Zirconium Diboride"; pp 53–67 in *Science of Ceramics*, Vol. 4, Edited by G. H. Stewart. The British Ceramic Society Academic Press, London, 1968.
[99]D. Kalish, E. V. Clougherty, and K. Kreder, "Strength, Fracture Mode, and Thermal Stress Resistance of HfB_2 and ZrB_2," *J. Am. Ceram. Soc.*, **52** [1] 30–6 (1969).
[100]J. R. Fenter, "Refractory Diborides as Engineering Materials," *SAMPE Quarter.*, **2**, 1–15 (1971).
[101]R. A. Andrievskii, L. A. Korolev, V. V. Klimenko, A. G. Lanin, I. I. Spivak, and I. L. Taubin, "Effect of Zirconium Carbide and Carbon Additions on Some Physicomechanical Properties of Zirconium Diboride," *Powder Metall. Metal Ceram.*, **19** [2] 93–4 (1980).
[102]D. Kalish and E. V. Clougherty, "Densification Mechanisms in High-Pressure Hot-Pressing of HfB_2," *J. Am. Ceram. Soc.*, **52** [1] 26–30 (1969).
[103]A. Bellosi, F. Monteverde, D. D. Fabbriche, and C. Melandri, "Microstructure and Properties of ZrB_2-Based Ceramics," *J. Mater. Proc. Man. Sci.*, **9** [2] 156–70 (2000).
[104]J. J. Melendez-Martinez, A. Dominguez-Rodriquez, F. Monteverde, C. Melandri, and G. de Portu, "Characterisation and High Temperature Mechanical Properties of Zirconium Boride-Based Materials," *J. Eur. Ceram. Soc.*, **22**, 2543–9 (2002).
[105]G. A. Meerson and A. F. Gorbunov, "Activated Sintering of Zirconium Boride," *Inorg. Mater.*, **4**, 267–70 (1968).
[106]F. Monteverde, S. Guicciardi, and A. Bellosi, "Advances in Microstructure and Mechanical Properties of Zirconium Diboride Based Ceramics," *Mater. Sci. Eng. A*, **A346**, 310–9 (2003).
[107]E. V. Clougherty, R. J. Hill, W. H. Rhodes, and E. T. Peters, "Research and Development of Refractory Oxidation-Resistant Diborides, Part II, Volume II. Processing and Characterization," AFML-TR-68-190 (DTIC AD-866558), January, 1970.
[108]W. H. Rhodes, E. V. Clougherty, and D. Kalish, "Research and Development of Refractory Oxidation-Resistant Diborides, Part II, Volume IV. Mechanical Properties," AFML-TR-68-190 (DTIC AD-865809), January 1970.
[109]F. Monteverde, A. Bellosi, and S. Guicciardi, "Processing and Properties of Zirconium Diboride-Based Composites," *J. Eur. Ceram. Soc.*, **22** [3] 279–88 (2002).
[110]A. Bellosi and F. Monteverde, "Ultra-Refractory Ceramics: The use of Sintering Aids to Obtain Microstructure Control and Properties Improvement"; pp. 787–92 in *Euro Ceramics VIII—Part 2, Vols. 264–268, Key Engineering Materials*, Edited by H. Mandal, and L. Öveçoglu. Trans Tech Publications Ltd., Switzerland, 2004.
[111]F. Monteverde and A. Bellosi, "Effect of the Addition of Silicon Nitride on Sintering Behaviour and Microstructure of Zirconium Diboride," *Script. Mater.*, **46** [3] 223–8 (2002).
[112]F. Monteverde and A. Bellosi, "Beneficial Effects of AlN as Sintering Aid on Microstructure and Mechanical Properties of Hot-Pressed ZrB_2," *Adv. Eng. Mater.*, **5** [7] 508–12 (2003).
[113]A. Chamberlain, W. Fahrenholtz, G. Hilmas, and D. Ellerby, "Characterization of Zirconium Diboride–Molybdenum Disilicide Ceramics"; pp. 299–308 in *Ceramic Transactions, Vol. 153, Advances in Ceramic Matrix Composites IX*, Edited by N. P. Bansal, J. P. Singh, W. M. Kriven, and H. Schneider. Am. Ceram. Soc., Westerville, OH, 2003.
[114]D. Sciti, L. Silvestroni, and A. Bellosi, "Fabrication and Properties of HfB_2–$MoSi_2$ Composites Produced by Hot Pressing and Spark Plasma Sintering," *J. Mater. Res.*, **21** [6] 1460–6 (2006).
[115]A. Bellosi, F. Monteverde, and D. Sciti, "Fast Densification of Ultra-High-Temperature Ceramics by Spark Plasma Sintering," *Int. J. Appl. Ceram. Technol.*, **3** [1] 32–40 (2006).
[116]M. Gasch, D. Ellerby, E. Irby, S. Beckman, M. Gusman, and S. Johnson, "Processing, Properties and Arc Jet Oxidation of Hafnium Diboride/Silicon Carbide Ultra High Temperature Ceramics," *J. Mater. Sci.*, **39** [19] 5925–37 (2004).
[117]F. Monteverde and A. Bellosi, "Microstructure and Properties of an HfB_2–SiC Composite for Ultra High Temperature Applications," *Adv. Eng. Mater.*, **6** [5] 331–6 (2004).
[118]F. Monteverde, "Beneficial Effects of an Ultra-Fine α-SiC Incorporation on the Sinterability and Mechanical Properties of ZrB_2," *Appl. Phys. A*, **82**, 329–37 (2006).
[119]I. G. Talmy, J. A. Zaykoski, M. M. Opeka, and A. H. Smith, "Properties of Ceramics in the System ZrB_2–Ta_5Si_3," *J. Mater. Res.*, **21** [10] 2593–9 (2006).
[120]F. Monteverde, D. D. Fabbriche, and A. Bellosi, "Zirconium Diboride-Based Composites"; pp. 961–4 in *Euro Ceramics VII—Part 2, Vols. 206–213, Key Engineering Materials*. Trans Tech Publications Ltd., Switzerland, 2002.
[121]F. Monteverde and A. Bellosi, "Efficacy of HfN as Sintering Aid in the Manufacture of Ultrahigh-Temperature Metal Diborides–Matrix Ceramics," *J. Mater. Res.*, **19** [12] 3576–85 (2004).
[122]V. Medri, F. Monteverde, A. Balbo, and A. Bellosi, "Comparison of ZrB_2–ZrC–SiC Composites Fabricated by Spark Plasma Sintering and Hot-Pressing," *Adv. Eng. Mater.*, **7** [3] 159–63 (2005).
[123]F. Monteverde and A. Bellosi, "Development and Characterization of Metal-Diboride-Based Composites Toughened With Ultra-Fine SiC Particulates," *Solid State Sci.*, **7**, 622–30 (2005).
[124]R. L. Coble and H. A. Hobbs, "Sintering," pp. 82–100 in *Investigation of Boride Compounds for Very High Temperature Applications, NTIS Report AD 428006*, Edited by L. Kaufman, and E. V. Clougherty. Federal Scientific and Technical Information, Springfield, VA, 1973.
[125]P. S. Kisliy and O. V. Zaverukha, "Theory and Technology of Sintering, Thermal, and Chemicothermal Treatment Processes," *Powder Metall. Metal Ceram.*, **9** [7] 549–51 (1970).
[126]H. R. Baumgartner and R. A. Steiger, "Sintering and Properties of Titanium Diboride Made From Powder Synthesized in a Plasma-Arc Heater," *J. Am. Ceram. Soc.*, **67** [3] 207–12 (1984).
[127]H. Pastor, "Metallic Borides: Preparation of Solid Bodies—Sintering Methods and Properties of Solid Bodies"; Chapter C.XIV, pp. 454–493 in *Boron and Refractory Borides*, Edited by V. I. Matkovich. Springer-Verlag, New York, NY, 1977.
[128]G. A. Meerson and A. F. Gorbunov, "Activated Sintering of Zirconium Boride," *Inorg. Mater.*, **4**, 267–70 (1968).
[129]B. Cech, P. Olivierus, and J. Sejbal, "Sintering of Zirconium Boride With Activating Additions," *Powder Metall.*, **8** [15] 142–51 (1965).
[130]P. S. Kisliy, M. A. Kuzenkova, and O. V. Zaveruha, "On the Sintering Process of Zirconium Diboride With Tungsten," *Phys. Sintering*, **3** [1] 29–44 (1971).
[131]V. M. Gropyanov, "Effect of Dispersion on Powder Sintering," *Refractories*, **34**, 769–75 (1969).
[132]O. Kida and Y. Segawa. U.S. Patent 4,636,481, January 13, 1987.
[133]O. Kida and Y. Segawa. U.S. Patent 4,678,759, July 7, 1987.
[134]M. Quabdesselam and Z. A. Munir, "The Sintering of Combustion Synthesized Titanium Diboride," *J. Mater. Sci.*, **22** [5] 1799–807 (1987).
[135]D. Sciti, S. Guicciardi, and A. Bellosi, "Properties of a Pressureless-Sintered ZrB_2–$MoSi_2$ Ceramic Composite," *J. Am. Ceram. Soc.*, **89** [7] 2320–2 (2006).
[136]A. L. Chamberlain, W. G. Fahrenholtz, and G. E. Hilmas, "Pressureless Sintering of Zirconium Diboride," *J. Am. Ceram. Soc.*, **89** [2] 450–6 (2006).
[137]W. G. Fahrenholtz, G. E. Hilmas, A. L. Chamberlain, and J. W. Zimmermann, "Processing and Characterization of ZrB_2-Based Monolithic and Fibrous Monolithic Ceramics," *J. Mater. Sci.*, **39** [19] 5951–7 (2004).
[138]H. Lee and R. F. Speyer, "Pressureless Sintering of Boron Carbide," *J. Am. Ceram. Soc.*, **86** [9] 1468–73 (2003).
[139]S. Prochazka and R. M. Scanlan, "Effect of Boron and Carbon on Sintering of SiC," *J. Am. Ceram. Soc.*, **58** [1–2] 72 (1975).
[140]G.-J. Zhang, Z.-Y. Deng, N. Kondo, J.-F. Yang, and T. Ohji, "Reactive Hot Pressing of ZrB_2–SiC Composites," *J. Am. Ceram. Soc.*, **83** [9] 2330–2 (2000).
[141]F. Monteverde, "Progress in the Fabrication of Ultra-High-Temperature Ceramics: "In Situ" Synthesis, Microstructure and Properties of a Reactive Hot-Pressed HfB_2–SiC Composite," *Comp. Sci. Tech.*, **65**, 1869–79 (2005).
[142]A. L. Chamberlain, W. G. Fahrenholtz, and G. E. Hilmas, "Low Temperature Hot Pressing of Zirconium Diboride Ceramics by Reactive Hot Pressing," *J. Am. Ceram. Soc.*, **89** [12] 3638–45 (2006).
[143]W.-W. Wu, G.-J. Zhang, Y.-M. Kan, and P.-L. Wang, "Reactive Hot Pressing of ZrB_2–SiC–ZrC Ultra High-Temperature Ceramics at 1800°C," *J. Am. Ceram. Soc.*, **89** [9] 2967–9 (2006).
[144]I. G. Talmy, J. A. Zaykoski, and M. A. Opeka, "Properties of Ceramics in the ZrB_2/ZrC/SiC System Prepared by Reactive Processing," *Ceram. Eng. Sci. Proc.*, **19** [3] 105–12 (1998).
[145]M. Nygren and Z. Shen, "On the Preparation of Bio-, Nano- and Structural Ceramics and Composites by Spark Plasma Sintering," *Solid State Sci.*, **5** [1] 125–31 (2003).
[146]W. Feng, P. Xiong, L. Yu, Y. Zheng, and Y. Xia, "Phase Evolution and Microstructure Characteristics of Ultrafine Ti(C,N)-Based Cermet by Spark Plasma Sintering," *Int. J. Refr. Metals Hard Mat.*, **22** [2–3] 133–8 (2004).
[147]B. Basu, T. Venkateswaran, and D.-Y. Kim, "Microstructure and Properties of Spark Plasma-Sintered ZrO_2–ZrB_2 Nanoceramic Composites," *J. Am. Ceram. Soc.*, **89** [8] 2405–12 (2006).
[148]F. Monteverde, C. Melandri, and S. Guicciardi, "Microstructure and Mechanical Properties of an HfB_2+30 vol% SiC Composite Consolidated by Spark Plasma Sintering," *Mater. Chem. Phys.*, **100** [2–3] 513–9 (2006).
[149]F. Monteverde, "Ultra-High Temperature HfB_2–SiC Ceramics Consolidated by Hot-Pressing and Spark Plasma Sintering," *J. Alloys Comp.*, **428** [1–2] 197–205 (2007).
[150]N. L. Okamoto, M. Kusakari, K. Tanaka, H. Inui, M. Yamaguchi, and S. Otani, "Temperature Dependence of Thermal Expansion and Elastic Constants of Single Crystals of ZrB_2 and the Suitability of ZrB_2 as a Substrate for GaN Film," *J. Appl. Phys.*, **93** [1] 88–93 (2003).
[151]E. D. Case, J. R. Smyth, and O. Hunter, "Grain-Size Dependence of Microcrack Initiation in Brittle Materials," *J. Mater. Sci.*, **15**, 149–53 (1980).
[152]M. K. Ferber, P. F. Becher, and C. B. Finch, "Effect of Microstructure on the Properties of TiB_2 Ceramics," *J. Am. Ceram. Soc.*, **66** [1] C2–4 (1983).
[153]A. Rezaie, W. G. Fahrenholtz, and G. E. Hilmas, "Effect of Hot Pressing Time and Temperature on the Microstructure and Mechanical Properties of ZrB_2–SiC," *J. Mater. Sci.* DOI 10.1007/s10853-006-1274-2.
[154]S. R. Levine, E. J. Opila, M. C. Halbig, J. D. Kiser, M. Singh, and J. A. Salem, "Evaluation of Ultra-High Temperature Ceramics for Aeropropulsion Use," *J. Eur. Ceram. Soc.*, **22**, 2757–67 (2002).
[155]G.-J. Zhang, M. Ando, J. F. Yang, T. Ohji, and S. Kanazaki, "Boron Carbide and Nitride as Reactants for In Situ Synthesis of Boride-Containing Ceramic Composites," *J. Euro. Ceram. Soc.*, **24**, 171–8 (2004).
[156]S. Zhu, W. G. Fahrenholtz, and G. E. Hilmas, "Influence of Silicon Carbide Particle Size on the Microstructure and Mechanical Properties of Zirconium Diboride–Silicon Carbide Ceramics," *J. Euro. Ceram. Soc.*, **27** [4] 2077–83 (2007).
[157]J. J. Cleveland and R. C. Brandt, "Grain Size/Microcracking Relations for Pseudobrookite Oxides," *J. Am. Ceram. Soc.*, **61** [11–12] 478–81 (1978).
[158]E. L. Kern, D. W. Hamil, H. W. Deam, and H. D. Sheets, "Thermal Properties of Silicon Carbide from 20 to 2000 deg," *Mater. Res. Bull.*, [4] S25–32 (1969).

Proceedings of the International Conference on Silicon Carbide—1968. Edited by R. C. Marshall, J. W. Faust, C. E. Ryan. Pergamon Press, Oxford, 1969.
[159]M. W. Barsoum, "Thermal Stress and Thermal Properties," pp. 488–492 in *Fundamentals of Ceramics*. McGraw-Hill Companies, New York, NY, 1997.
[160]J.-S. Kim, "Spark Plasma Sintering of Molybdenum Dilisicide," *Key Eng. Mater.*, **287**, 160–5 (2005).
[161]D. E. Wiley, W. R. Manning, and O. Hunter, "Elastic Properties of Polycrystalline TiB_2, ZrB_2 and HfB_2 From Room Temperature to 1300°K," *J. Less-Common Metals*, **18**, 149–57 (1969).
[162]C. K. Jun and P. T. B. Shaffer, "Elastic Modulus of Dense Silicon Carbide," *Mater. Res. Bull.*, **7** [1] 63–70 (1972).
[163]M. Nakamura, S. Matsumoto, and T. Hirano, "Elastic Constants of $MoSi_2$ and WSi_2 Single Crystals," *J. Mater. Sci.*, **25** [7] 3309–13 (1990).
[164]H. Kodama and T. Miyoshi, "Study of Fracture Behavior of Very Fine-Grained Silicon Carbide Ceramics," *J. Am. Ceram. Soc.*, **73** [10] 3081–6 (1990).
[165]S. Maloy, A. H. Heuer, J. Lewandowski, and J. Petrovic, "Carbon Additions to Molybdenum Disilicide: Improved High Temperature Mechanical Properties," *J. Am. Ceram. Soc.*, **74** [10] 2704–6 (1991).
[166]K. T. Faber and A. G. Evans, "Crack Deflection Processes—I. Theory," *Acta Metall.*, **31** [4] 565–76 (1983).
[167]K. T. Faber and A. G. Evans, "Crack Deflection Processes—II. Experiment," *Acta Metall.*, **31** [4] 577–84 (1983).
[168]W. J. Clegg, K. Kendall, N. McN. Alford, T. W. Button, and J. D. Birchall, "A Simple Way to Make Tough Ceramics," *Nature (London)*, **357**, 455–7 (1990).
[169]D. Kovar, B. H. King, R. W. Trice, and J. W. Halloran, "Fibrous Monolithic Ceramics," *J. Am. Ceram. Soc.*, **80** [10] 2471–87 (1997).
[170]W. D. Kingery, "Factors Affecting Thermal Stress Resistance of Ceramic Materials," *J. Am. Ceram. Soc.*, **38** [1] 3–15 (1955).
[171]D. P. H. Hasselman, "Thermal Shock by Radiation Heating," *J. Am. Ceram. Soc.*, **46** [5] 229–34 (1963).
[172]D. P. H. Hasselman, "Thermal Stress Resistance Parameters for Brittle Refractory Ceramics," *Bull. Am. Ceram. Soc.*, **49**, 1033–7 (1970).
[173]W. R. Buessem, "Thermal Shock Testing," *J. Am. Ceram. Soc.*, **38** [1] 15–7 (1955).
[174]E. V. Clougherty, E. T. Peters, and D. Kalish, "Diboride Materials, Candidates for Aerospace Applications"; pp. 297–308 in *Materials and Processes for the 1970's – Vol. 15. Proceedings of the 15th SAMPE Symposium, April 29–May 1, 1969*, Los Angeles, CA, Western Periodicals Co., North Hollywood Hills, CA, 1969.
[175]D. Kalish, E. V. Clougherty, and K. Kreder, "Strength, Fracture Mode, and Thermal Stress Resistance of HfB_2 and ZrB_2," *J. Am. Ceram. Soc.*, **52** [1] 30–6 (1969).
[176]F. Monteverde, "Progress in the Fabrication of Ultra-High-Temperature Ceramics: "In Situ" Synthesis, Microstructure and Properties of a Reactive Hot-Pressed HfB_2-SiC Composite," *Comp. Sci. Tech.*, **65**, 1869–79 (2005).
[177]Y.-H. Koh, H.-W. Kim, H.-E. Kim, and J. W. Halloran, "Thermal Shock Resistance of Fibrous Monolithic Si_3N_4/BN Ceramics," *J. Eur. Ceram. Soc.*, **24**, 2339–47 (2004).
[178]L. Kaufman, E. V. Clougherty, and J. B. Berkowitz-Mattuck, "Oxidation Characteristics of Hafnium and Zirconium Diboride," *Trans. Metall. Soc. AIME*, **239** [4] 458–66 (1967).
[179]J. B. Berkowitz-Mattuck, "High-Temperature Oxidation III. Zirconium and Hafnium Diborides," *J. Electrochem. Soc.*, **113** [9] 908–14 (1966).
[180]W. C. Tripp and H. C. Graham, "Thermogravimetric Study of the Oxidation of ZrB_2 in the Temperature Range of 800° to 1500°C," *J. Electrochem. Soc.*, **118** [7] 1195–9 (1971).
[181]H. C. Graham, H. H. Davis, I. A. Kvernes, and W. C. Tripp, "Microstructural Features of Oxide Scales Formed on Zirconium Diboride Materials"; pp. 35–48 in *Ceramics in Severe Environments*, Edited by W. W. Kriegel, and H. Palmour III. Plenum Press, New York, 1971.
[182]A. K. Kuriakose and J. L. Margrave, "The Oxidation Kinetics of Zirconium Diboride and Zirconium Carbide at High Temperatures," *J. Electrochem. Soc.*, **111** [7] 827–31 (1964).
[183]C. B. Bargeron, R. C. Benson, R. W. Newman, A. N. Jette, and T. E. Phillips, "Oxidation Mechanisms of Hafnium Carbide and Hafnium Diboride in the Temperature Range 1400°C and 2100°C," *J. Hopkins APL Tech. Digest*, **14** [1] 29–36 (1993).
[184]F. Monteverde and A. Bellosi, "Oxidation of ZrB_2-Based Ceramics in Dry Air," *J. Electrochem. Soc.*, **150** [11] B552–9 (2003).
[185]R. J. Irving and I. G. Worsley, "The Oxidation of Titanium Diboride and Zirconium Diboride at High Temperatures," *J. Less Common Metals*, **16**, 103–12 (1968).
[186]W. G. Fahrenholtz, "The ZrB_2 Volatility Diagram," *J. Am. Ceram. Soc.*, **88** [12] 3509–12 (2005).
[187]A. Bongiorno, C. J. Först, R. K. Kalia, J. Li, J. Marschall, A. Nakano, M. M. Opeka, I. G. Talmy, P. Vashishta, and S. Yip, "A Perspective on Modeling Materials in Extreme Environments: Oxidation of Ultra-High Temperature Ceramics," *MRS Bull.*, **31** [5] 410–8 (2006).
[188]W. C. Tripp, H. H. Davis, and H. C. Graham, "Effect of an SiC Addition on the Oxidation of ZrB_2," *Ceram. Bull.*, **52** [8] 612–6 (1973).
[189]E. V. Clougherty, R. L. Pober, and L. Kaufman, "Synthesis of Oxidation Resistant Diboride Composites," *Trans. Metall. Soc. AIME*, **242** [6] 1077–82 (1968).
[190]Q. N. Nguyen, E. J. Opila, and R. C. Robinson, "Oxidation of Ultrahigh Temperature Ceramics in Water Vapor," *J. Electrochem. Soc.*, **151** [10] B558–62 (2004).
[191]F. Monteverde, "The Thermal Stability in Air of Hot-Pressed Diboride Matrix Composites for Uses at Ultra-High Temperature," *Corr. Sci.*, **47**, 2020–33 (2005).
[192]A. Rezaie, W. G. Fahrenholtz, and G. E. Hilmas, "Evolution of Structure During the Oxidation of Zirconium Diboride-Silicon Carbide in Air up to 1500°C," *J. Eur. Ceram. Soc.*, **27** [6] 2495–2501 (2007).
[193]E. J. Opila and M. C. Halbig, "Oxidation of ZrB_2–SiC," *Ceram. Eng. Sci. Proc.*, **22** [3] 221–8 (2001).
[194]A. L. Chamberlain, W. G. Fahrenholtz, and G. E. Hilmas, "Oxidation of ZrB_2–SiC Ceramics Under Atmospheric and Reentry Conditions," *Refract. Appl. Trans.*, **1** [2] 1–8 (2005).
[195]V. A. Lavrenko, A. D. Panasyuk, T. G. Protsenko, V. P. Dyatel, E. S. Lugovskaya, and E. I. Egorova, "High Temperature Reactions of Materials of the ZrB_2–$ZrSi_2$ System With Oxygen," *Poroshkovaya Metall.*, **6** [234] 56–8 (1981).
[196]W. G. Fahrenholtz, "Thermodynamic Analysis of ZrB_2–SiC Oxidation: Formation of a SiC–Depleted Region," *J. Am. Ceram. Soc.*, **90** [1] 143–148 (2007).
[197]A. Rezaie, W. G. Fahrenholtz, and G. E. Hilmas, "Oxidation of Zirconium Diboride-Silicon Carbide at 1500°C in a Low Partial Pressure of Oxygen," *J. Am. Ceram. Soc.*, **89** [10] 3240–5 (2006).
[198]D. Sciti, M. Brach, and A. Bellosi, "Oxidation Behavior of a Pressureless Sintered ZrB_2–$MoSi_2$ Ceramic Composite," *J. Mater. Res.*, **20** [4] 922–30 (2005).
[199]E. Opila, S. Levine, and J. Lorincz, "Oxidation of ZrB_2- and HfB_2-based Ultra-High Temperature Ceramics: Effect of Ta Additions," *J. Mater. Sci.*, **39** [19] 5969–77 (2004).
[200]I. G. Talmy, J. A. Zaykoski, M. M. Opeka, and S. Dallek, "Oxidation of ZrB_2 Ceramics Modified With SiC and Group IV–VI Transition Metal Borides"; pp. 144–53 in *High Temperature Corrosion and Materials Chemistry III*, Edited by M. McNallan, and E. Opila. The Electrochemical Society, Pennington, NJ, 2001.
[201]J. D. Bull, D. J. Rasky, and J. C. Karika, "Stability Characterization of Diboride Composites Under High Velocity Atmospheric Flight Conditions"; pp. T1092–1106 in *Advanced Materials: Meeting Economic Challenges, Proceedings of the 24th International SAMPE Technical Conference, October 20–22, 1992, Toronto, Canada*, Edited by M. Rosenow, T. J. Reinhart, F. H. Froes, and R. A. Cull. Society for the Advancement of Material and Process Engineering, Covina, CA. □

Bill Fahrenholtz is an Associate Professor of Ceramic Engineering at the University of Missouri-Rolla. He earned B.S. and M.S. degrees in Ceramic Engineering at the University of Illinois at Urbana-Champaign in 1987 and 1989, respectively. He completed his Ph.D. in Chemical Engineering at the University of New Mexico in 1992. From 1993 to 1999, Bill was a research assistant professor at UNM. Since 1999, he has been at UMR where he has received several campus-wide faculty excellence and teaching awards as well as a CAREER award from the National Science Foundation. He teaches undergraduate and graduate courses on thermodynamics as well as a required sophomore level laboratory on traditional ceramics. His research focuses on the processing and characterization of ceramics and ceramic-metal composites. He has current projects related to ultra-high temperature ceramics as well as the use of cerium oxide coatings for the corrosion protection of high-strength aluminum alloys. He has published over 50 papers on his work.

Greg Hilmas is an Associate Professor of Ceramic Engineering at the University of Missouri-Rolla. He earned B.S. in Materials Science and Engineering at the University of Minnesota, his M.S. degree in Ceramic Engineering at The Ohio State University, and his Ph.D. in Materials Science and Engineering from the University of Michigan in 1986, 1988, and 1993, respectively. From 1993 to 1994, Greg was a post-doctoral researcher at the University of Michigan. From 1995 to 1997, Greg was the Composite Materials Manager at Advanced Ceramics Research in Tucson, AZ. Since 1998, he has

been at UMR where he has received 10 campus-wide faculty excellence and teaching awards. In addition, Greg has received an R&D 100 award for the development of fibrous monolith materials for rock drill bit inserts for the petroleum drilling industry. He teaches undergraduate and graduate courses on composite materials and the thermal and mechanical properties of ceramics. His research focuses on the processing, microstructure and properties of ceramics and ceramic composites. He has current projects related to ultra-high temperature ceramics; high voltage, high-energy density capacitors; and rapid prototyping of ceramics. He has published over 50 papers on his work.

Inna Talmy is the Senior Research Ceramist and Group Leader of the Ceramic Science and Technology Group at NSWCCD. She joined the Laboratory in 1983. Inna received both her M.S. (1957) and Ph.D. (1965) degrees in Ceramic Science and Engineering from the Mendeleev Institute of Chemical Technology in Moscow, Russia. Previously, she worked at the Institutes of Chemical Technology in Moscow and Prague, Czechoslovakia. Her primary research efforts are in dielectric ceramics, superconductors, non-oxide structural ceramics, and ceramic-matrix composites. Inna directed the development of celsian and phosphate ceramics as candidates for next generation tactical missile radomes. Currently, her research is focused on UHTC materials (such as ZrB_2–SiC and cermets) with improved oxidation and thermal stress resistance for hypersonic and strategic missile applications. Talmy's work has resulted in over 80 publications and 20 patents. Her work has been recognized with several awards from the U.S. Navy including a Meritorious Civilian Award, the Adolphus Dahlgren Award, a Science and Technology Excellence Award, and a NAVSEA Scientist of the Year Award.

James Zaykoski is a materials scientist in the Ceramic Science and Technology Group at NSWCCD, which he joined 1985. He received a B.S. (1985) in Materials Engineering from Wilkes University, and an M.S. (1988) and a Ph.D. (1994) in Materials Engineering from the University of Maryland. His research at NSWCCD has focused on optimized processing of carbon–carbon composites, toughening of ceramics, modeling of polymorphic phase transformations and gaseous diffusion, developing oxidation protection coatings and high-temperature ceramic-based adhesives, and developing non-oxide ceramics for structural applications in oxidizing environment. His work has resulted in 20 publications and nine patents. Jim received the NSWC Young Professional of the Year Award in recognition of his accomplishments.